



Assessing the performance of the seismic coda spectral factorization method the for the site effect estimation

Grendas Ioannis, Hollender Fabrice, Theodoulidis Nikolaos, Hatzidimitriou
Panagiotis, Bard Pierre-Yves and Perron Vincent

Work Package #4 "Site response"



AUTHORS		REVIEW		APPROVAL	
Name	Date	Name	Date	Name	Date
<i>GRENDAS Ioannis</i>	2022/06/09 	<i>MAIN Ian</i> <i>MARTIN Christophe</i>	YYYY/MM/DD	<i>Fabrice HOLLENDER</i> Public-access <input type="radio"/> SIGMA-2 restricted <input checked="" type="radio"/>	2022/06/09 

Document history

DATE	VERSION	COMMENTS
2020/05/13	1	<i>Original manuscript</i>
2022/06/09	2	<i>Account taken of the Scientific Council's comments.</i>

Executive summary

The reliability of a site-specific seismic hazard assessment is highly dependent on the quality of the soil response (or site effect) evaluation. There are several methods for estimating the site effect, either using numerical simulation tools or empirical approaches. One of the most widely used empirical methods is the so-called “Standard Spectral Ratio” (SSR) classical method (*Borcherdt, 1970*). This approach is based on a seismic event simultaneously being recorded on a reference station (rock site), considered to be amplification-free, and on a nearby station at the studied site. The main limitation of this method lies in the availability of a reference station relatively close to the studied site. Indeed, one important condition of the SSR method is that the distance between the reference and site stations must be at least 10 times smaller than the epicentral distance of the causative earthquakes. In some cases, it is not easy to have such a reference station close to the site station. This is for example the case in the context of large sedimentary basins (e.g. the Rhone valley in France). The method proposed by *Sèbe et al. 2018*, based on the spectral factorization of the source time function (STF) of an earthquake using earthquake coda wave record, can potentially allow circumventing this limitation.

The latter method theoretically allows performing an, SSR-like, site effect analysis using reference stations at a large distance from the study site. The spectral factorization method is quite complex and involves advanced signal processing approaches. It firstly requires the “stationarization” of the seismic Coda (evaluation of the Coda amplitude decay and attenuation factor removal) and then the estimation of the minimum phase wavelet, equivalent to the seismic Source Time Function (STF). The STF can be determined for a single event-station pair. The STF obviously includes information on the magnitude and kinematics of the source, but also contains the signature of the site effect of the study site. If this station is considered to be free of any amplification (reference station), then the STF characterizes only the intrinsic characteristics of the source. STFs calculated for the same earthquake but for different stations can therefore be used as the classical SSR method, determining the site spectral amplification (called Transfer Function, TF) at a target site in relation to the reference site (free of amplification). Since STFs are distance-independent, theoretically, there is no restriction in distance between ‘reference’ and ‘site’ stations. At this study, the validity of the above SSR-like site effect analysis is investigated and the applicability of this TF estimation technique, are evaluated.

The spectral factorization method was adapted and tested for this study, performing SSR-like applications based on a high-quality dataset from the Ionian Sea zone. This zone is one of the most seismic areas in the Euro-Mediterranean region. The dataset integrates 24 sites and 89 seismic events, with $3.9 \leq ML \leq 5.1$. In this data set, four stations (CKWP, ITC1, VSK1 and AST1, ~15 to 65 km distances between each other) can be considered as reference rock sites and two stations (CK0 and CK83, surface and bottom common-borehole stations) can be used, in conjunction with CKWP, to compute classical-SSR (the distance between CK0 and CKWP is about 0.4 km). Results obtained by classical-SSR and by spectral-factorization-SSR are satisfactorily comparable. Hence, the potential applicability of the spectral factorization technique is validated by the results of this study.

1 Introduction

The main object of this study focuses on the establishment of a relatively simple technique of Transfer Function (TF) determination at a site, in relation to a distant reference site. This TF determination is based on real earthquake data and more specifically to coda wave seismic records. The presented technique follows two analysis steps. At the first one the Source Time Function (STF) of an individual earthquake is separately estimated at two recording sites, based on the methodology introduced by *Sebe et al. 2018*, applied on the coda wave part of an earthquake record. At the second one the Fourier Spectra of the two STFs are compared each other “revealing” their relative spectral amplification. In case where one of them is a site without spectral amplification (reference) due to the surface geology, the non-reference site TF can be retrieved by their STF spectral ratio. The second step is similar to the process commonly applied in the Standard Spectral Ratio (SSR) technique (*Borcherdt, 1970*). In this last technique, the spectral ratio of the S-wave strong motion records of an earthquake at two adjacent stations, where one is a reference station, can be considered as the TF of the non-reference one. This can be considered due to the common STF and to the similar path attenuation. Regarding the technique established and examined in this study, the only conditions required for its application is 1) to consider a common seismic source, for the two examined coda wave records, without being necessary the restrictive pre-condition of the adjacent station, 2) The similar coda excitation factor and average shear wave velocity of the path. This seems being true when reference-target site distance reaches even the ~30 km, while strong indications for the right use of this technique at extended reference-target site distance, after excitation factor correction, constitute keystone for further study.

The first, workable goal of the below study is to estimate the STFs of several earthquakes in western Greece recorded at several sites in this high seismicity area. The second, but substantial goal is to determine the TFs by comparing the computed STFs at the examined sites to the corresponding ones at four, distant from each other, reference sites (rock installed stations). The potential stability of the TFs at each site and the agreement of the average TFs, computed in relation to the four different reference sites is going to reasonably support the reliable applicability of the proposed technique. This applicability will be confirmed by comparing these TFs results with the corresponding ones computed from SSR at some station (where are available), or other methods (e.g. Generalized Inversion Technique, HVSR). During this effort and due to the fact that the STF estimation methodology (*Sebe et al. 2018*), which is the first step of the TF estimation technique, basically refers to reference sites (without spectra amplification), the applicability of this methodology to non-reference sites has to be also studied. We address the last issue in this study, testing the degree of the expected stability of the computed TFs from the several examined earthquakes at each site separately. The results provide strong indications of TFs stability and supports the concept that the average TFs for several earthquakes can be used to infer the STFs in areas where there is no close reference site, and hence be used to infer the relative site response, despite the large spatial separation, at least in the cases examined here.

It's worth noting that a new developed - available - STF computation MATLAB algorithm, was developed for this study based on the one of *Sebe et al. 2018*, but applying a few alternative but reasonable procedures, analytically mentioned in the below analysis. These procedures are referring to: 1) the reliable coda wave signal detection through the initial Signal to Noise Ratio process, 2) The different strategy followed on the steps of the attenuation factor analysis 3) The different minimum phase STF computation process, 4) the correction of the low frequency STF part, as well as to its scaling, concluding to the seismic moment, M_0 computation 5) the uncertainties propagation to the STF, M_0 and TF estimation. These procedures were considered trying to achieve the most valid defined STFs, in order to conclude to reliable TF results. By this way, the potential of the proposed technique, can be significantly determined, as possible.

Before the application of the TF estimation technique, the basic step analysis of the STF estimation methodology that were partially revised from the pioneer study of *Sebe et al. 2018*, as well as the earthquake data examined at this study for their STFs, are firstly presented below.

2 Data

Seismic records of 105 earthquakes ($M_L=3.9-5.1$), were initially examined for the computation of their Source Time Function (STF), in order to further study the site effects at the recorded sites. These earthquakes were located on western Greece (**Figure 1**), at the time period between 9/8/2015 – 26/11/2019,

The record sites (**Figure 1, Appendix A**) refer to the locations of the 18 ITSAK accelerometric network (<http://www.itsak.gr>) stations and to the 6 accelerometric ARGOnet stations (5, in a borehole to depths: 0, 6, 15, 40, 83 meters, at the center of Koutavos sedimentary basin and 1 rock installed, on the edge of the basin) (*Theodoulidis et al. 2018*). All the stations used are broad band accelerometers.

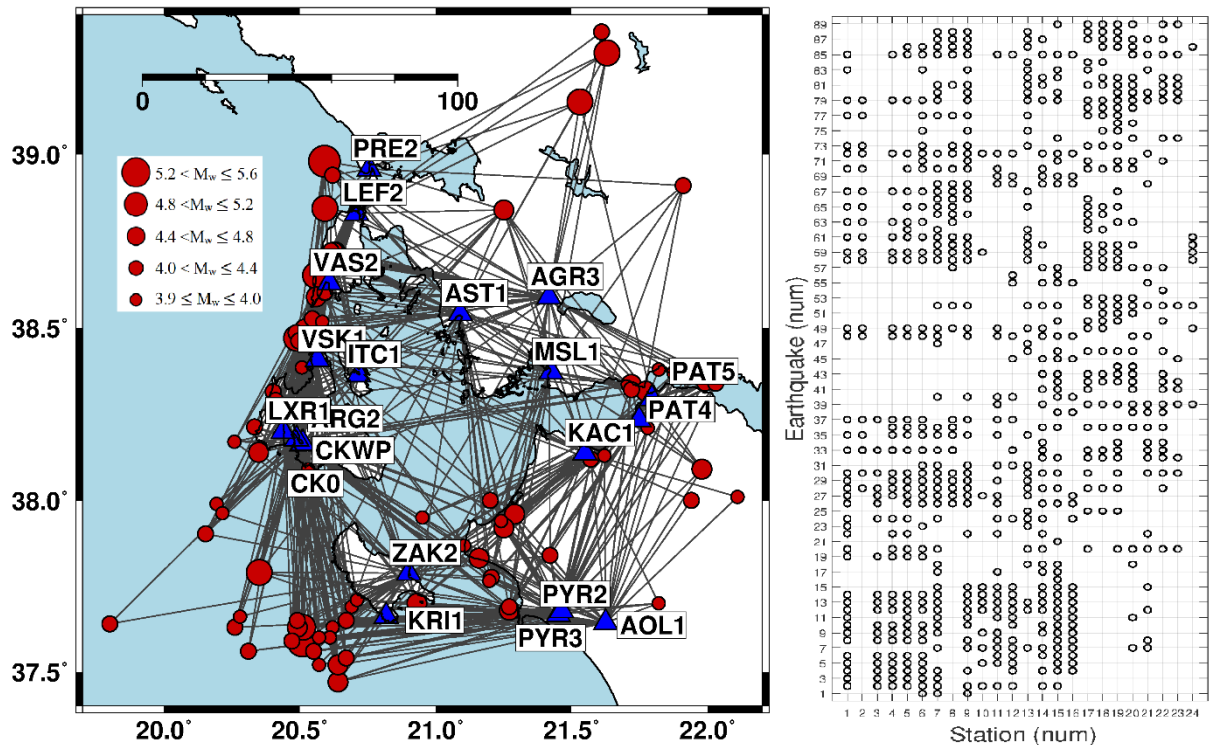


Figure 1. (a) The studied area (west Greece-Ionian Sea). 747 pairs of earthquakes-station for which coda wave records were examined in this study. 89 earthquakes (epicenters: red cycles) and 24 accelerometer stations (blue triangles, <http://www.itsak.gr>). (b) The distribution of the computed STF of each earthquake at each station (according to Appendix A and B)

The collected seismic records were examined for a reliable 60 sec required coda wave window as mentioned below. The arrival time of the coda waves was considered as two times the S-wave arrival time, t_c ($t_c=2 \cdot t_s$), (*Aki, 1969*) but being greater than 30 seconds after the earthquake origin time and lower than 70 sec of it, too. The first criterion was applied in order to avoid as possible surface waves and the very early coda waves that could probably be affected by the strong motion “tail” at sites where the amplification is significant. This affection was confirmed by observations at several cases in the examined dataset. The second criterion was applied so that the examined 60 sec coda time windows at several sites from the same earthquake presenting at least a 30% overlap in time (e.g. the case of having two coda windows at 30 to 90 sec and 70 to 130 sec from the earthquake origin time).

Finally, 739 STFs were computed corresponding to 89 earthquakes (**Figure 1, Appendix B**), where it is obvious that STFs from each earthquake are not estimated to each site. This is either due to the lack of the corresponding seismic record at some sites, or because of the lack of a reliable 60 sec coda wave window at least for the frequency range: 0.5 to 3 Hz, investigated in this study. This frequency range, that is under the engineering seismology

interest, was chosen as the minimum, for which the STF could be investigated. Further study could reduce this range so that to retrieve even a minimum “information” about the STF.

After the signal reliability detection, all the acceleration seismic records were integrated by applying a Butterworth (2-order) High-Pass filter at 0.05 Hz (the low frequency limit of the instruments), so that to retrieve the corresponding velocity records and to use them as input at the STF computation algorithm, developed in this study.

3 STF estimation methodology

The Source Time Function estimation analysis studied here, follows a methodology introduced in seismology by *Sebe et al. 2018*. This methodology is applied to seismic records theoretically retrieved from reference stations (assuming no amplification). Briefly, this methodology is based on the following three main facts: 1) According to *Wiener-Khinchin* theorem, the Power Spectrum of the STF wavelet (attenuation (corresponding to the kind of record examined: velocity, or acceleration) is equal to the Fourier Transform of the autocorrelation, computed from a suitable stationary waveform. 2) This stationary coda waveform can be theoretically achieved after removing the suitable attenuation factor from the coda wave record, in the time domain. This factor is controlled by a coda wave attenuation model for which the frequency dependent coda quality factor has to be firstly determined. 3) The minimum phase wavelet computed from the STF Fourier Amplitude Spectrum, (equal to the square root of the STF Power Spectrum, in displacement), can be consider as the STF of the earthquake, as explained and approved by *Sebe et al. 2018*.

As mentioned above, this methodology is basically applied for earthquakes recorded at a reference site where no spectral amplifications affect the seismic motion. Ideally, the application of the above mentioned three facts can lead to a well determined STF at a reference site, assuming that the examined attenuation model satisfactorily simulates the real attenuation process. However, in “real life” the analysis followed for each one of the above three facts, usually includes limitations and uncertainties in computations, or diverges from some ideal pre-conditions in methodology. This can affect the STF estimation. The reliable part of the signal in comparison to the noise, or the adequacy of the attenuation model to simulate perfect the attenuation process, are some of these limitations. Even the site effect existence can insert uncertainties to the STF estimation. The investigation of the last factor constitutes the main objective of this study. Below, the limitations and uncertainties in STF estimation are tried to be controlled at each step of the examined methodology (**Figure 2**), concluding to a its valid application and aiming to the reliable TFs determination.

3.1 Signal Reliability

The determination of the reliable part of the coda wave record is a pre-condition for the valid applicability of the coda wave analysis. This determination is achieved for each component separately, in the frequency and in time domains. According to *Aki, (1969)* the initial examined coda wave record window is defined, from a start time, (t_c) of $2 \cdot t_s$ (t_s , the S-wave travel time) after the earthquake origin time, either up to the end of the record, or up to the appearance of a new earthquake record. Here, the t_c was chosen as it mentioned above at the Data sub-chapter. It is worth noting that the coda wave arrival time still remains an under-study issue, ranging between $2 \cdot t_s$ and $3 \cdot t_s$ (among others: *Rautian and Khalturin, 1978*), so that to avoid surface waves, as possible. Below in this study, at the application of the methodology, a suitable strategy of the examined coda wave window determination, is presented, supporting the applicability of it. To ensure the best choice of the coda wave record, for the examined frequency range and trying to avoid noise, it is necessary to characterize the minimum Signal to Noise ratio. Here, this is characterized by two particular procedures.

The first one is that the noise used for the SNR process is sampled from a long-time window (e.g. 120 sec) before the P-wave arrival (**Figure 3a**). This window is considered to be representative of the average noise level dominating the site in time close to the earthquake arrival. The geometric mean of the Fourier Amplitude (FA) spectra (**Figure 3b**), of several consecutive noise windows in time (**Figure 3a**), plus its one standard deviation is used to estimate this average noise level. Finally, coda wave (Signal) Fourier Amplitudes 1.5 times greater than this average noise level ($\text{SNR}(f) > 1.5$), in frequency domain, is considered to be a reliable signal for the purposes of this study (**Figure 3c**).

The second feature of this SNR process was applied aiming to better investigate the reduction of the signal amplitude in time, detecting the reliable part of coda both on frequency and time domain. Consecutive sliding time windows, of several increased duration (**Figure 3a**) were used in order to better test all the examined frequency range and its changes into the time. It is obvious that the use of long-time consecutives coda windows cannot precisely catch small changes at high frequency amplitudes in time, while short-time widows cannot “see” the existing low frequency waves. For this reason, both short and long windows are used to detect high and low frequency amplitude changes in time. For example here 10, 20, 40, 80 sec and so on (up to the length of the coda wave record) half overlapped, coda windows were initially used to compute FA for the frequency ranges: $0.1 - (f_s/2)$ Hz (f_s sampling frequency), 0.05-0.1 Hz, 0.025-0.05 Hz, 0.0125-0.025 Hz and so on, respectively.

Regarding the second feature of the SNR process an extra strict criterion was used for even more valid computations. Four (4) cycles of signal duration were used as the lowest reliable frequency limiting factor (*Perron et al. 2018*) on the Fast Fourier Transform (FFT) computation. Thus, the final frequency ranges studied for the above coda wave durations in this study was: $0.4 - (f_s/2)$ Hz, 0.2-0.4 Hz, 0.1-0.2 Hz, 0.05-0.1 Hz and so on, respectively. The same time windows were examined also for the average noise (**Figure 3a**) as mentioned above, for the same frequency ranges (**Figure 3b**), in order to finally estimate the reliable part of coda wave through the SNR process (**Figure 3c**).

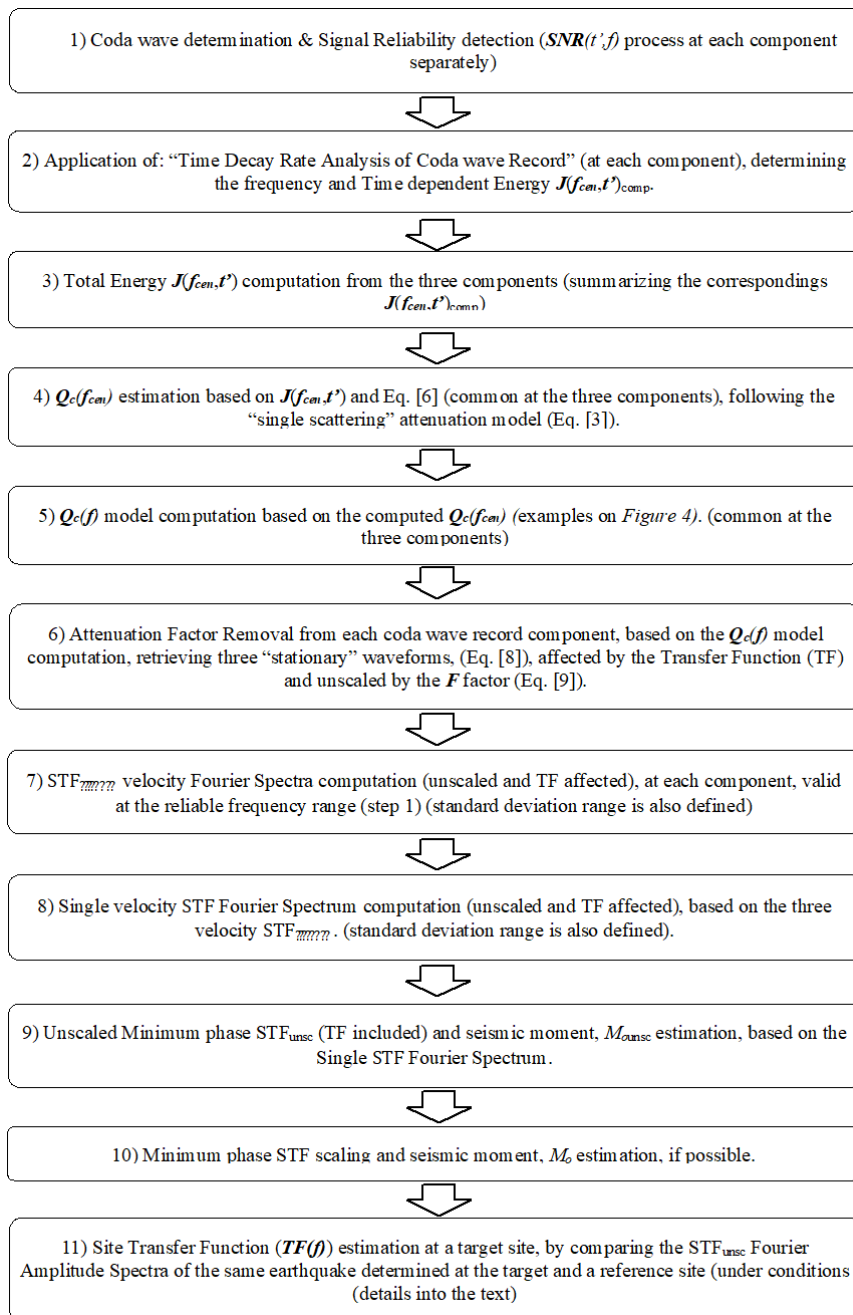


Figure 2. The flowchart of the STF computation algorithm developed at this study based on the one developed by *Sebe et al. 2018*, including the last step of TF(f) estimation analysis.

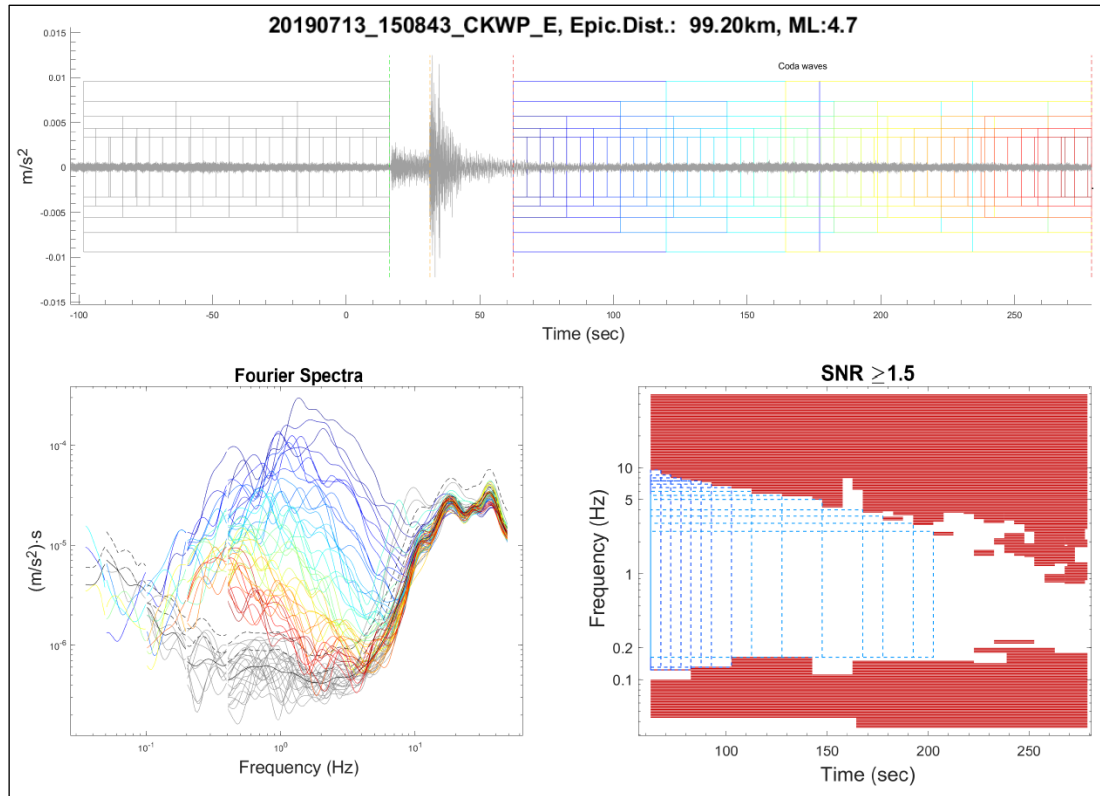


Figure 3. (a) The acceleration record (“E-W” component) of an earthquake at the station “CKWP”. Noise and coda wave record examined window are depicted (grey and multi-colors, respectively). (b) The Fourier Amplitudes of the corresponding window of **Fig. 3(a)**. Geometrical mean spectrum (G.M.S) (solid black line), G.M.S. plus its one standard deviation (dashed line), and the final noise level used (1.5 times greater than the second one). (c) The coda wave Fourier Amplitudes per real record time, with SNR < 1.5 (red points) and the reliable corresponding amplitudes (white). The dashed line cyan windows represent the several potential examined time windows for different frequency ranges.

The minimum required length of the coda wave window as well as the required frequency range constitute the two factors defining the final reliable signal window that will be studied for the STF. Reasonably, when the required coda time window is increased, the reliable Fourier Amplitude frequency range is normally decreased, as at the example of **Figure 3c**. At this figure with blue dashed lines the maximum coda time windows that can be considered for different maximum frequency ranges, are defined. In this study, a minimum frequency range from 0.5 Hz up to 2.5 Hz, was required for all the examined records. Also, a long coda wave time window of 60 sec, was chosen to be examined, in order to study the capability of the methodology to reliably compute the low frequency plateau of the STF. This plateau is necessary for the seismic moment (M_0) estimation and to the valid STF determination. Based on the above SNR process, the maximum frequency range that can be entirely studied for a 60 sec window, is finally detected. At the example of **Figure 3c** this maximum frequency range is 0.09 – 5.5 Hz. Finally, for the three components of motion for an earthquake – station pair with the same time window and the same frequency range must be examined.

3.2 Attenuation model

The removal of the attenuation factor from the coda wave record aims to reduce this record to a zero epicentral distant stationary waveform, which is necessary for the STF detection. In this study the attenuation factor is based on the so-called “single scattering” attenuation model of body waves (*Aki and Chouet, 1975*). This model is based on the study case of the impulsive spherical radiation of the total energy at an elastic infinite medium, where scatterers exist. As a result, seismic waves are backscattered to the receivers. Coda waves recognized first by (*Aki,*

1969 and Aki and Chouet, 1975), are considered as the superposition of these scattered seismic wavelets (mainly body S-waves, among others: Aki, 1980a) on randomly distributed inhomogeneities in the lithosphere. At the single scattering model, the backscattering process is assumed to be relatively weak, since each wavelet is considered as single time backscattered. In terms of energy the relation between the Power Spectral Density (PSD), $R_{ij}(f)$ of a velocity coda wave record for one component, at a station j corresponding to an earthquake i , can be described by the following formula in frequency domain (Sebe et al. 2018):

$$R_{ij}(f) = W_i(f) \cdot E_c(f) \cdot |A_c(f, t')|^2 \cdot N_j(f) \quad [1]$$

where the second and the third term of the product correspond to the attenuation factor, while the first, $W_i(f)$ and the last term $N_j(f)$, are related to the source and Site effect factors, respectively. Before the analysis of the attenuation factor, it is reminded that the real site spectral amplification, $S_j(f)$ is actually expressed in terms of amplitudes, where it is: $N_j(f) = S_j^2(f)$, ($N_j(f)$ is expressed in energy domain), as well as that the PSD of the Seismic Source, $W_i(f)$ (under the assumption of an isotropic source radiation), is given by:

$$W_i(f) = \frac{|\hat{\Omega}_i(f)|^2}{10\pi\rho\beta^5} \quad [2]$$

where the $\hat{\Omega}_i(f)$ corresponds to the STF Fourier Spectrum in velocity domain. The denominator of the above ratio constitutes the seismic source scaling factor (Vassiliou and Kanamori, 1982). This factor is controlled by the density ρ and the shear wave velocity β at the medium close to the seismic source.

Regarding attenuation factor, in terms of energy (Eq. [1]), the single scattering attenuation model, used in this study, is controlled (in frequency domain), by the product of the excitation factor $E_c(f)$ with the factor $|A_c(f, t')|^2$:

$$|A_c(f, t')|^2 = \frac{1}{(v_s \cdot t')^\eta} e^{-\frac{2\pi f t'}{Q_c(f)}} \quad [3]$$

where t' , is the travel time of the signal, v_s , the average shear wave velocity considered for the area of interest and $Q_c(f)$ is the frequency dependent quality factor for the coda waves.

The first part of Eq. [3] controls the wave geometrical spreading loss of energy, where for the single scattering model it is considered $\eta = 2$ (Aki and Chouet, 1975, Sato, 1977, Sato et al. 2012). The second part controls the loss of energy due to both anelastic (intrinsic) attenuation and scattering of the body S- waves. This kind of attenuation is referred to the elastic properties of the medium that are related to its heterogeneous “character” (among others: Soham and Abhishek, 2016) due to velocity variabilities and to the presence of geological structures (e.g. faults, folds etc.). The last two factors of attenuation (anelasticity of the medium and scattering) are studied together being initially impossible to simultaneously separate them at this study.

The excitation factor $E_c(f)$ (Eq. [1]), included to the single scattering attenuation model, indirectly indicates the amount of scatterers at the crust of interest area, controlling the degree of scattering constituting a travel time, t' independent scaling factor of attenuation.

Following Sebe et al. 2018 it is:

$$E_c(f) = \frac{1}{\pi \cdot l(f)} \quad [4]$$

where $l(f)$ is the frequency dependent mean free path, characterizing the distribution of the scatterers. Mean free path is an a priori unknown “free” parameter that describes the wave propagation providing information about the tectonic statement (Sato, 1978).

Under the assumption of the reference site (no spectral amplification), *Sebe et al. 2018* refer to the well-approached exponential model of crustal heterogeneities distribution, supported by *in situ* observations (*Dolan et al. 1998*) and suitable analysis measurements (*Gusev and Abubakirov, 1996*). Based on the above, they theoretically consider that for the single scattering model, where the attenuation factor $A_c(f, t')$ “cares” about the exponential decay of coda wave amplitudes, the mean free path could also be consider as frequency independent where:

$$l(f) = l \Leftrightarrow E_c(f) = E_c \quad [5]$$

Thus, the stationary (corrected by $A_c(f, t')$) coda waveform can be considered as the convolution of the repetition of STF wavelet (in velocity) with the square root of coda excitation term $E_c(f) = E_c$ (stable), in time domain, since $E_c(f)$ refers to energy.

3.3 Quality factor estimation

The coda quality factor, Q_c computation is based on the time decay rate analysis of coda wave envelopes, outlined by *Aki and Chouet, (1975)*. This analysis follows the principal of energy conservation between source and receiver, at continuous wave arrival times, based on the single scattering attenuation model and it is described below according to *Margerin et al. (1999)*. Initial goal of the analysis is the independent estimation of coda quality factors, $Q_c(f_{cen.})$ corresponding to central frequencies, $f_{cen.}$. In this study 25 $f_{cen.}$, equally distributed on logarithmic scale between 0.06 and 30 Hz where chosen. Following the steps of analysis, for frequency windows of width equal to 2/3 of these central frequencies the coda wave record (separately at each component) is initially bandpass filtered (**Figure 3**). The energy $J(f_{cen.}, t')$ of consecutive signal (coda filtered) envelopes, of duration equal to the central period ($T_{cen} = 1/f_{cen.}$), 1.5 sec time step and with middle time the, arrival t' time, is computed. The sum of the square of the filtered signal Amplitudes at each signal envelope, corresponds to this energy $J(f_{cen.}, t')$. Consequently, after logarithmization of Eq. [1], and taking into account Eq. [3], it is:

$$\ln[J(f_{cen.}, t') \cdot t'^{\eta}] = V(f) - \frac{2\pi f_{cen.} t'}{Q_c(f_{cen.})} \quad [6]$$

for each filtered signal envelope corresponding to t' arrival time. V factor includes all the time, t' independent factors of Eq. [1]. ($W_i(f)$, E_c , $N(f)$). The same process is applied on noise record so that to detect only the reliable coda wave part from which Q_c will be finally computed. The geometric mean value of filtered noise record plus its one standard deviation is considered as the average noise level and a Signal to Noise ratio (SNR) greater than 1.5 is the reliability signal criterion (**Figure 3a**). At this step, instead of computing the quality factors, $Q_c(f_{cen.})$ for each component separately, we choose to sum the corresponding energies $J(f_{cen.}, t')$ only at the common reliable part of the signal envelopes of the three components and finally to determine the common $Q_c(f_{cen.})$, by a least square analysis (L-S) (**Figure 3b**) at the one-degree polynomial of Eq. [6], for each central frequency, $f_{cen.}$ (**Figure 4**). Standard deviations of $Q_c(f_{cen.})$ are also determined. It is worth noting that the L-S analysis is implemented only if the duration of the examined corrected signal is greater than 10 cycles of the corresponding T_{cen} ($1/f_{cen.}$) (e.g. for $f_{cen.} = 1$ Hz, 10 sec minimum signal), with a minimum threshold on 30 sec and a maximum of 180 sec. These empirical limits were taken into account based on our observations, in order: 1) to conclude to reliable and robust slopes ($Q_c(f_{cen.})$) and 2) to avoid distant enough, regional attenuation affections.

The stationarization process of coda waveform, which is a necessary step to STF estimation, is achieved through the attenuation factor (Eq. [2]) removal in time domain, as described by *Sebe et al. 2018*. At this step the frequency dependent quality factor $Q_c(f)$ (Eq. [2]) must be determined for all the required frequencies of the inverse-Fourier process. Thus, a computation formula in order to reproduce the required $Q_c(f)$ is used as explained below, based on the computed $Q_c(f_{cen.})$. Regarding the way of $Q_c(f)$ estimation, the bellow function (*Aki, 1980b, Singh and Hermann, 1983*):

$$Q_c(f) = Q_c \cdot f^a \quad [7]$$

is usually applied so that to express the exponential variability of quality factor with frequencies mainly for $f > 1$ Hz (among others: *Aki, 1980b*, *Dainty, 1981*, *Hatzidimitriou, 1993*, *Margerin et al. 1998*, *Tselentis, 1998*, *Sato et al. 2012*, *Sebe et al. 2018*). However, as outlined by *Herraiz and Espinosa, (1986)*, based on *Sato, (1982)* computations and on Aki's conjecture (*Aki, 1980a*), the theoretical quality factors, $Q_c(f)$ present also an exponential increase for the lowest frequencies (below ~ 1 Hz). In this study, the $Q_c(f)$ required for the attenuation factor (Eq. [2]) removal in time domain, were computed following the decay of Q_c up to ~ 1 Hz, expressed by Eq. [7], but also the increase from ~ 1 Hz to lower frequencies. Thus, trying to empirical model this $Q_c(f)$ "behavior", a 3rd, or a 2nd degree polynomial between $\ln(Q_c(f_{cen}))$ and $\ln(f_{cen})$, or sometime a 1st degree (same as Eq. [7]), was used, as it is shown at the characteristic examples of **Figure 5**. At this regression analysis, standard deviations of $Q_c(f_{cen})$ are taken into account and finally the standard deviation of the computed polynomial is used at the STF computation process for its better and more reliable and valid estimation. **Figure 6** presents all the estimated $Q_c(f)$ models for each earthquake at each station.

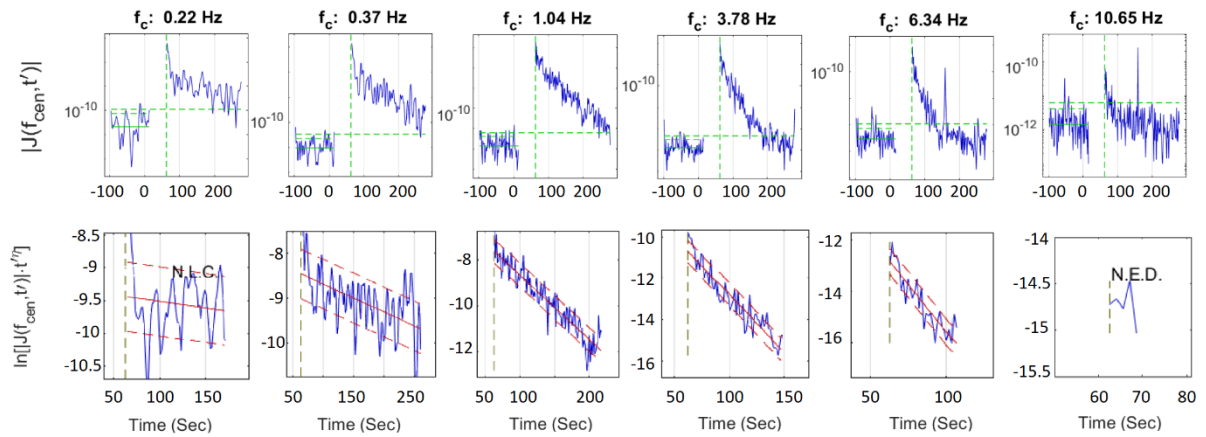


Figure 4. (a) (Upper line) Examples of the $|J(f_{cen}, t')|$ energy (blue line) at each time t' of the band-passed signal (coda wave and noise) for 6 central frequencies (f_{cen}) (for the record of **Figure 3a**). S-wave arrival time, t_s , Average Noise Level (A.V.L.), the A.V.L. + standard deviation and the final examined noise level (vertical green and horizontal solid and dashed lines, respectively), are also depicted. (b) (bottom line) The $\ln(|J(f_{cen}, t')| t')$ quantity (Eq. [6]), corresponding to **Figure 4a** (but common for the three components), computed only for the coda wave part. The least square analysis (red solid line) with its standard deviation (red dashed line) are depicted, where N.L.C. and N.E.D. indicate Non-Linear Correlation and Not Enough Data according to the criteria mentioned into the text.

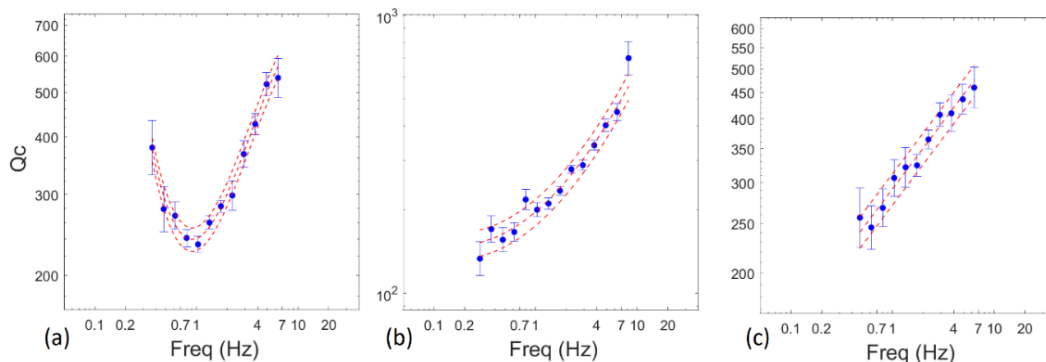


Figure 5. Three characteristic examples of the $Q_c(f)$ computation model based on a regression analysis (red dashed lines) of: 3rd, 2nd, and 1st order polynomial (Fig. (a), (b) and (c), respectively), between $\ln(Q_c(f_{cen}))$ and $\ln(f_{cen})$ (details into the text). Standard deviation of the determined line is also computed. **Figure 5a** corresponds to the $Q_c(f_{cen})$ from **Figure 4**.

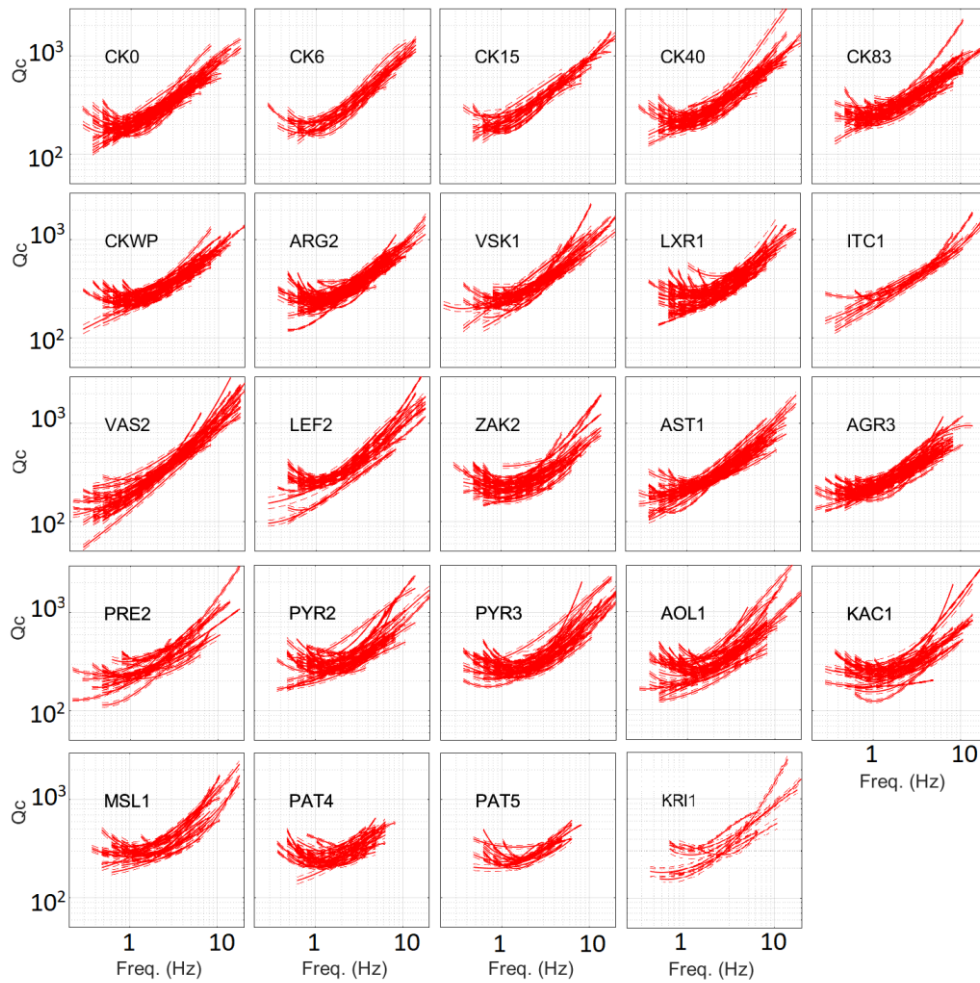


Figure 6. The $Q_c(f)$ models (red lines) and their standard deviation range (red dashed lines) computed from each earthquake coda wave record to each site one of the 24 sites (**Figure 1**) (same scaling at all the 24 sub-Figures).

3.4 Attenuation Removal

After the quality factors are determined, the attenuation factor correct the coda wave record at each component, is applied concluding to a stationary coda waveform (**Figure 7a**). More specifically, 3 different stationary coda waveforms are determined for each component, for the three different $Q_c(f)$ models (the average and two for the standard deviation range, e.g. **Figure 5**). These waveforms are theoretically “reduced” to zero hypocentral distance. In this study this removal is based on the well-defined and studied by *Sebe et al. 2018* process. For this reason, we do not refer to details about this process. Briefly, the attenuation factor removal is achieved by deconvolving the minimum phase wavelet formed by the frequency dependent part of Eq. [1], from the coda waveform. In fact, the deconvolution is applied for all the moving, tapered by Hanning window, in consecutive 60 sec, time windows (zero padded where it is needed), and the stationary waveform is created by the median value in time of each corrected coda window.

Since this process is applied in the time based on the frequency domain, using a deconvolution process applied in frequency domain, the quality factor must be computed for all the frequencies defined at the inverse Fourier Transform (FT) for a 60 sec window. Thus, as the polynomial relating $\ln(Q_c(f_{cen}))$ and $\ln(f_{cen})$, is determined as explained above (**Figure 5**), the $Q_c(f)$ for the FT required frequencies are computed. It must be noted that for frequencies f , below the $f_{cen(low)}$ that corresponds to the lowest determined $Q_c(f_{cen(low)})$, it is $Q_c(f) = Q_c(f_{cen(low)})$.

3.5 Unscaled STF estimation at a reference station

Based on the relation of the coda waveform PSD to the Source, attenuation and Site factors (Eq. [1]) and after the removal of the frequency and lapse-time dependent attenuation factor ($|A_c(f, t')|^2$, Eq. [2]) from the coda wave record, the PSD, $C_{ij}(f)$ of the corrected stationary coda waveform (**Figure 7a**), is given by:

$$C_{ij}(f) = W_i(f) \cdot E_c \cdot \frac{1}{v_s^\eta} \cdot N_j(f) \quad [8]$$

At the above equation the factors: $\frac{1}{10\pi\rho\beta^5}$ (Eq. [2]), $\frac{1}{\pi l}$ (Eq. [4, 5]) and $\frac{1}{v_s^\eta}$ (Eq. [3]) are frequency and time independent. For this reason, they can be considered as the Seismic Source “scaling” factors and from now their product will be called as “**F**”. Thus Eq. [8] can be written as:

$$C_{ij}(f) = |\hat{\Omega}_i(f)|^2 \cdot N_j(f) \cdot F \quad [9]$$

The STF(t) estimation methodology proposed by *Sebe et al. 2018* initially assuming for no site spectral amplification ($S_j(f) = 1 = S_j^2(f) = N_j(f)$) is based on the above equation relating a stationary coda waveform to the seismic source, as well as to the *Wiener-Khinchin* theorem supporting that the PSD of the STF, ($|\hat{\Omega}_i(f)|^2 \cdot F$, Eq. [9]), is equal to the Fourier Transform of the normalized autocorrelation of this stationary waveform (**Figure 7a**). However, this process cannot be applied straight on a displacement waveform but at the available velocity one. Thus, the directly computed STF PSD at each component corresponds to velocity and not to the real STF in displacement. However, based on these PSDs, the minimum phase wavelet, STF(t)_{min}, in displacement, which is considered equal to the real STF(f) (*Sebe et al. 2018*), (when STF(t) is a non-complicated time function) can be computed following the process analytically presented below.

At this study, velocity earthquake waveforms were used as initial input data from which the stationary coda waveforms are computed (Eq. [9]), (**Figure 7a**). The autocorrelation functions are computed (**Figure 7b**) for three, 25% overlapped, 40 sec windows (**Figure 7a**), applying the cross correlation of the signal with itself, normalized by the number of points. Only, the 1/3 of the positive and the negative part, which is considered as the reliable part of the autocorrelation functions is tapered by a Parzen window (**Figure 7c**), removing the late lag noise. Thereafter, according to the *Wiener-Khinchin* theorem, mentioned direct above, the relation between the Fourier Amplitude (FA) spectrum of the normalized autocorrelation to the PSD of the STF (Eq. [9]) in velocity, into the MATLAB developed in this study algorithm, is:

$$\text{FA}[\text{acorr}_{\text{norm}}(t)] = \text{PSD}[STF(t)] \Leftrightarrow \text{abs}\{\text{fft}[\text{acorr}_{\text{norm}}(t)]\} \cdot dt = \text{abs}\{\text{fft}[STF(t)]\}^2 \cdot dt/N \quad [10]$$

where N is the number of autocorrelation function points as well as of the expected STF(t) and dt is the time step. **fft** is the function describing the Fast Fourier Transform.

Here it must be noted that since the PSD of the stationary waveform includes the **F** factor (Eq. [9], $N(f)=1$ at the reference station hypothesis examined in this chapter), the stationary waveform includes the \sqrt{F} factor and consequently its autocorrelation function and its Fourier Amplitude Spectrum (Eq. [10]) will include the F (\sqrt{F}^2) factor. Thus, finally the investigated PSD of STF(t) at Eq. [10], is actually unscaled for the **F** factor and it is:

$$\text{abs}\{\text{fft}[\text{acorr}_{\text{norm}}(t)]\} \cdot dt = \mathbf{F} \cdot \text{abs}\{\text{fft}[STF(t)]\}^2 \cdot dt/N \quad [11]$$

Taking into account that the autocorrelation function is normalized by N as mentioned above, Eq. [11] can be analyzed as:

$$\text{abs}\{\text{fft}[\text{acorr.}(t)/N]\} = \mathbf{F} \cdot \text{abs}\{\text{fft}[S\dot{T}F(t)]\}^2/N \Leftrightarrow \text{abs}\{\text{fft}[\text{acorr.}(t)]\}/N = \mathbf{F} \cdot \text{abs}\{\text{fft}[S\dot{T}F(t)]\}^2/N \Leftrightarrow$$

$$\Leftrightarrow \sqrt{\mathbf{F}} \cdot \text{abs}\{\text{fft}[S\dot{T}F(t)]\} = \text{abs}\{\text{fft}[\text{acorr.}(t)]\}^{1/2} \Leftrightarrow \sqrt{\mathbf{F}} \cdot S\dot{T}F(t)_z = \text{ifft}\{\text{abs}\{\text{fft}[\text{acorr.}(t)]\}^{1/2} \cdot dt\} \quad [12]$$

$$\Leftrightarrow \sqrt{\mathbf{F}} \cdot S\dot{T}F(t)_z = \text{ifft}\{\text{abs}\{\text{fft}[\text{acorr.}(t)]\}^{1/2}\} = S\dot{T}F(t)_{z_{\text{unsc}}}$$

where $S\dot{T}F(t)_z$, corresponds to the zero phases velocity Source Time Function wavelet since at the above equation the imaginary part of Fourier Transform, for each frequency, is unknown and it is considered equal to zero for convenience in computations. The $S\dot{T}F(t)_{z_{\text{unsc}}}$ corresponds to the unscaled $S\dot{T}F(t)_z$ for $\sqrt{\mathbf{F}}$ (Eq. [9]) (e.g. **Figure 7d**), in velocity.

Three $S\dot{T}F(t)_{z_{\text{unsc}}}$ are computed for the three 40 sec coda stationary windows. These $S\dot{T}F(t)_{z_{\text{unsc}}}$ are low-Pass filtered (4th, or higher order Butterworth filter) at the higher reliable frequency (SNR process estimated), removing the detected high frequency noise.

The minimum phase wavelets of the $S\dot{T}F(t)_{z_{\text{unsc}}}$ were computed (**Figure 7e**), and their average one, as well as its standard deviation, are computed based on the geometric mean of their Fourier Amplitudes (**Figure 7f**). In fact, the minimum phase computation of the velocity $S\dot{T}F(t)_{z_{\text{unsc}}}$, at this step, is not necessary and is implemented only for visual reasons. Instead of this, the “average” unscaled zero phases wavelet, $S\dot{T}F(t)_{z_{\text{unsc}}}$, could be also computed, having the same Fourier Amplitudes to the minimum phase one and from which the corresponding unscaled displacement $STF(t)_{z_{\text{unsc}}}$ can be estimated at the next step. In algorithm developed in this study, a minimum phase wavelet is computed using the “rceps” MATLAB function.

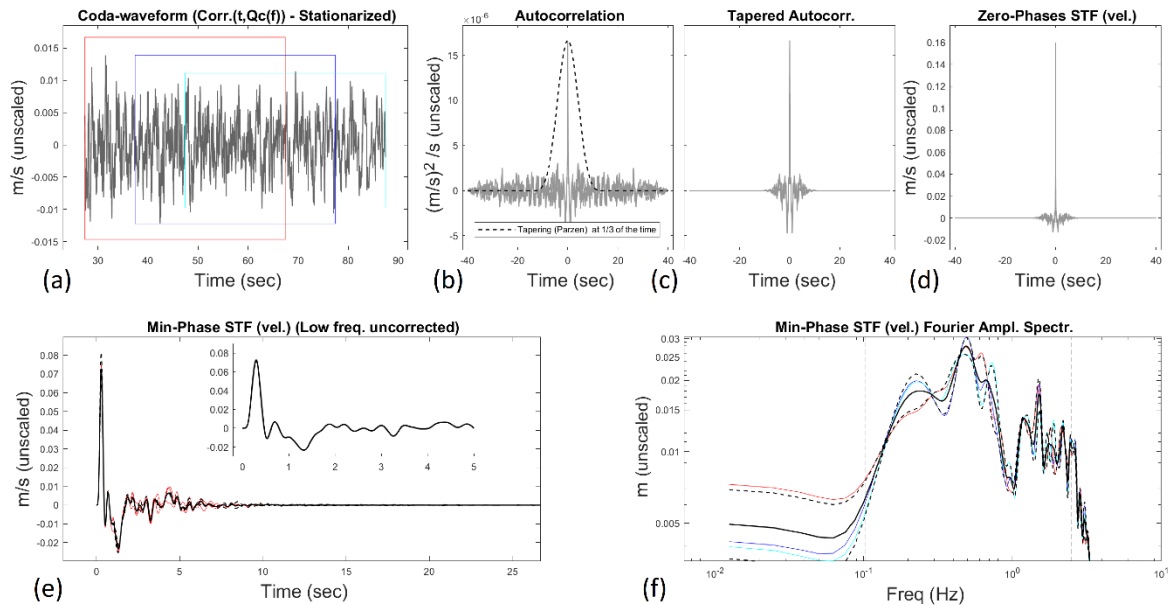


Figure 7. (a) An example of a 60 sec corrected (stationary) velocity coda waveform of an earthquake (20151117_123756, ML= 4.5, Epic. Dist. = 38km) recorded at a rock site (ITC1.). (b) The 3 normalized autocorrelations of the 40 sec time windows (25% overlapped) (red, blue, cyan) of Fig. 5(a) and the applied tapering (Parzen window, dashed line). (c) The 3 smoothed by tapering autocorrelation functions (T.A.F.) of Fig. 5(b). The 3 zero-phases wavelets computed from the T.A.F. of Figure 5(c) (details into the text). (e) The 3 minimum phase wavelets (M.F.W.) of the Fig. 5(d) wavelets (red), and their average one (black). (g) The 3 Fourier spectra of the Fig.(e) M.F.W, (colors correspond to Fig. (a)), their geometric mean Spectrum (solid black) and their standard deviation in log scale (dashed black). The vertical back dashed lines indicate the reliable part of the spectrum as studied by SNR process (**Figure 3**).

Before the computation of the minimum phase displacement $STF(t)_{min}$, the common unscaled (Eq. [12]) minimum phase velocity $\dot{STF}(t)_{min_{unsc}}$ of the three components it must be determined. This is achieved in two steps: 1) For the three stationary waveforms computed at each component for the three examined attenuation factors, the average unscaled (Eq. [12]) $\dot{STF}_c(t)_{min_{unsc}}$ and its standard deviation are computed, based on the geometric mean of their Fourier Amplitudes and on their corresponding standard deviation as explained above. 2) The common unscaled (Eq. [12]) velocity $\dot{STF}(t)_{min_{unsc}}$ of the three components (EW, NS, Z), is computed based on the geometrical contribution of their Fourier Amplitudes (e.g. **Figure 8a**):

$$FA(f)_{STF} = \sqrt{FA(f)_{EW}^2 + FA(f)_{NS}^2 + FA(f)_Z^2} \quad [13]$$

and recomputing the minimum phase wavelet (e.g. **Figure 8b**) in velocity. The corresponding standard deviation range is computed taking also into account the propagated standard deviation of the FAS at each component, according to Eq. [13]. It is worth noting that also at these two steps the minimum phase computation is not necessary to be applied and the zero-phase assumption can be instead included to the velocity $\dot{STF}(t)$ computations. Finally, the unscaled from factor \sqrt{F} (Eq. [9]), minimum phase $STF(t)_{min}$ in displacement (e.g. **Figure 8c**) is estimated by integrating once the corresponding velocity $\dot{STF}(t)_{unsc}$ (minimum or zero phase) and computing its minimum phase wavelet (“rceps” MATLAB function). At this step it must be noted that before integration a two-order High pass Butterworth filter at the low frequency limit (0.05 Hz), corresponding to the reliable part of the broad-band instrument, is applied. This filtering process is necessary in order to pass from velocity to displacement, without affections from the very low uncertain frequencies. By this way the corrected displacement Fourier Amplitudes are maintained equal to the corresponding velocity ones divided by the angular frequency, $\omega_k = 2\pi f_k$, for the k frequencies greater than 0.05 Hz. It is obvious that the frequency content of the STF can be reliable only up to the lowest frequency valid limit of the instrument.

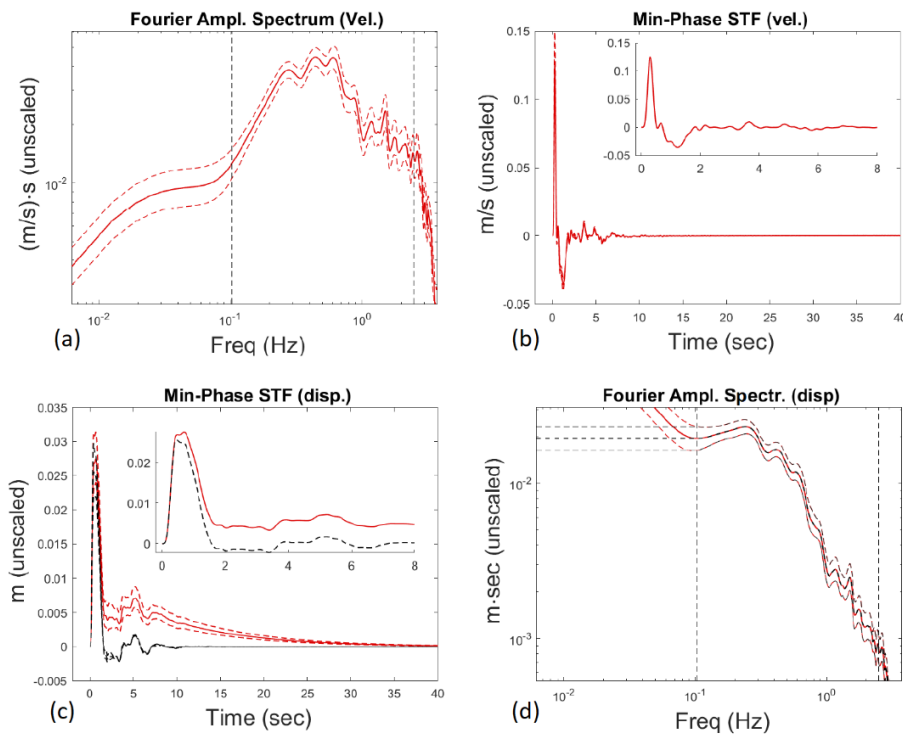


Figure 8. (a) The common unscaled (Eq. [12]) velocity STF FAS corresponding to the example of **Figure 5**. (b) The minimum phase velocity STF with FAS of Fig. a. (c) The unscaled (similar as Eq. [12]) minimum phase displacement STF after integration of the corresponding velocity one (Fig. b) (red line) and the corrected for the low frequency plateau (black line) (details into the text). (d) The FAS of the min. phase STF of Fig. c.

The computed unscaled minimum phase displacement $STF(t)_{min_{unsc}}$ includes the frequency independent source scaling factor \sqrt{F} (Eq. [9]), as the corresponding velocity once (Eq. [12]), since this constant factor is frequency and time independent.

Moreover, the $STF(t)_{min_{unsc}}$ is affected at low frequencies by noise as it can be observed at the examples of **Figure 8c,d**. This affection starts close to the lowest reliable frequency detected at the *a priori* “Signal to Noise Ratio” process, up to the zero frequency and it is propagated from the computed $STF(t)_{min}$ in velocity at each component (**Figure 7f**). Actually, noise “contaminates” the expected low frequency plateau of the $STF(t)_{disp}$ Fourier Amplitude Spectrum (FAS) (**Figure 8d**). In consequence this “contamination” affects the right computation of seismic moment, M_o ($M_o = FAS(0) = FAS_{STF}(f_{plateau})$, $f_{plateau}$ are the frequencies correspond to this FAS plateau) and the shape of the $STF(t)_{min_{unsc}}$ (**Figure 8c**). However, the reliable frequency part of the FAS_{STF} detected at the SNR process does not affected from the low frequency noise but only from the \sqrt{F} scaling factor.

Trying to correct for a valid $STF(t)_{min_{unsc}}$ (displacement), at a reference site (no amplification), so that its Fourier Amplitude Spectrum presenting a plateau at frequencies beyond the corner frequency, f_c ($f_c = 1/T_c$, T_c the rupture duration), if possible, a simple but practical strategy, mentioned below, is followed.

In cases where the reliable FAS_{STF} presents relevant stable values (“flat” shape) at low frequencies, it is considered that this part of the FAS belongs to the expected low frequency plateau of the $STF(t)_{min_{unsc}}$ FAS (e.g. **Figure 8d**). Based on this, the $FAS(f_{LR})$ value corresponding to the last reliable frequency, f_{LR} , detected from the SNR process, is considered as the stable value of this plateau up to the zero frequency. This value is also equal to the seismic unscaled for the factor constant \sqrt{F} (Eq. [9]), seismic moment, M_o , corresponding to the $FAS(0)$. Details about the F , scaling factor (Eq. [9]) definition are presented below, at: “STF scaling and M_o computation” subchapter. Finally, the valid unscaled STF correction is achieved by reducing all the low frequency, noise affected, Fourier Amplitudes up to the zero frequency and by recalculating the minimum phase wavelet of the corrected FAS (**Figure 8d**).

The computed unscaled $STF(t)_{min_{unsc}}$, after the above process application, corresponding to a reference site, is expected to be a positive wavelet as the one corresponding to the energy released at the seismic source.

Similar process is suggested to be applied for the minimum phase $STF(t)_{disp}$ estimation at non-reference sites as outlined below, but considering that the computed $STF(t)_{min_{unsc}}$, is site affected and it cannot be considered as the actually $STF(t)$.

3.6 Unscaled STF estimation at a non-reference station

Based on Eq. [9], in case of site Spectral amplification, $S(f)$ ($N(f) = S^2(f)$) existence, the above mentioned “STF” Fourier Spectra Amplitudes is expected being affected independently at each frequency by $S(f)$. Based on this and assuming the finite dimensions of the particular surface site geological conditions that affect the seismic waves, $S(f)$ should be reduced to one (no amplification) for the quite lower frequencies, depending on the site characteristics (e.g. shear wave velocity distribution, depth of the basin, etc). However, these “lower” frequencies are not initially known, but their expected no amplification values can be depicted as the stable FAS, that could correspond to the low frequency FAS plateau of the STF. Thus, in case where the well-defined low frequency FA of the $STF(t)$ (in displacement), indicate the low frequency plateau, then same correcting process applied at reference site (mentioned above in this study), can be followed. A corrected example of a $STF(t)$ computed at a non-reference site (sedimentary basin installed) is presented in **Figure 9**.

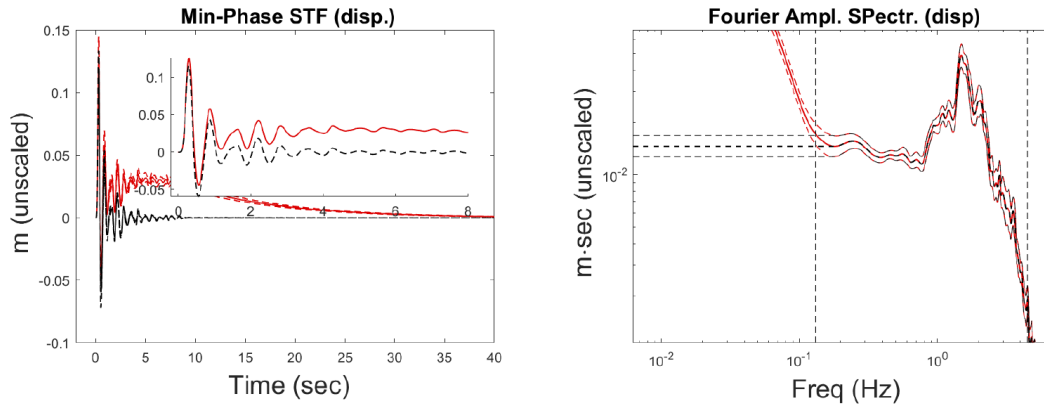


Figure 9. (a) An example of an unscaled (Eq. [9]) minimum phase STF_{disp} (site effect included) of an earthquake recorded at the “CK0” sedimentary basin installed site (uncorrected and corrected for the low frequency plateau, red and black line, respectively) and (b) their FAS.

3.7 STF scaling and M_o computation

After the unscaled $STF(t)_{min_{unsc}}$ (site effect included) estimation at an examined site and under the condition that the low frequency plateau of the determined STF is observed, the unscaled seismic moment by the $\sqrt{\mathbf{F}}$ factor (Eq. [9, 12]) can be also observed taking into account that the STF Fourier Amplitude at zero frequency is equal to the seismic moment, M_o . The simple Eq. [14] expresses this relation between the M_o and the unscaled M_o .

$$M_{o_{unsc}} = M_o \cdot \sqrt{\mathbf{F}} \quad [14]$$

However, the knowledge of the factor, \mathbf{F} and consequently the seismic moment, M_o , estimation, still remains an issue. Two computation strategies can be applied in determining the M_o .

The first one is simply based on the M_o scaling of an examined earthquake in comparison to a previous one located on the same area and recorded at the same station, for which the M_o is already computed from different methodology. Thus, from the unscaled computed $STF(t)$ and the known M_o of the second one earthquake, the $\sqrt{\mathbf{F}}$ factor can be computed from Eq. [14]. Finally, correcting the unscaled $STF(f)$ of the examined earthquake for this factor (reasonably considering that is similar, studying similar lapse time coda windows), its M_o can be computed from Eq. [14], too. It is obvious that this strategy could contribute to the seismic moment estimation of low magnitudes earthquakes for which the M_o cannot be computed from different methodologies.

The second one is based on an effort of direct computation of the scaling factor, $\sqrt{\mathbf{F}}$ (Eq. [9]). This could be achieved by using typical values controlling the density, ρ and the shear wave velocity, β at the medium close to the seismic source (Eq. [2]), the mean free path, l (Eq. [4]) and from the average shear wave velocity of the attenuation path, v_s (Eq. [3]). Although these parameters are unknown in absolute, several reasonable values can be considered in order to finally compute the average STF and seismic moment, M_o and their standard deviation.

More specifically, the commonly used average shear wave velocity, v_s at the upper crust is considered: 3.5 km/sec. Here reasonable v_s values from 3.0 km/sec to 4.0 km/sec are assumed, counting for the standard deviation range of the average STF. It is worth noting that based on Eq. [8], the maximum error of the average computed moment Magnitude, M_w , determined for $v_s=3.5$ km/s and corresponding to the reasonably assumed standard deviation range (3.0 – 4.0 km/s) of v_s , is ~ 0.0446 . This is defined based on the M_w difference between the extreme values of the standard deviation in comparison to the average considered one, from the following equation (*Hanks and Kanamori, 1979*):

$$\log_{10}(M_o) = 1.5M_w + 9.1 \quad [15]$$

where according to Eq. [14] it is:

$$\log_{10}(M_{o_{unsc}}) - \log_{10}(\sqrt{F}) = 1.5M_w + 9.1 \quad [16]$$

and finally, the moment magnitude, M_w is directly and independently related to the v_s value but also to the ρ , β and l (Eq. [4,5]) through the following equation:

$$\log_{10}(M_{o_{unsc}}) + \frac{\log_{10}(10\pi) + \log_{10}(\rho) + \log_{10}(\beta^5)}{2} + \log_{10}(v_s) = 1.5M_w + 9.1 \quad [17]$$

The same average and standard deviation range values (3.0-4.0 km/s) of shear wave velocities, β are considered for the medium close to the seismic source. In this case and also based on Eq. [17] the corresponding maximum error of the average computed moment Magnitude, M_w is ~ 0.1116 .

Following the same computation strategy and based on the commonly used and accepted density of the Earth's crust close to the faults ($\sim 2.8 \text{ gr/cm}^3$), values from 2.5 to 3.1 gr/cm^3 were considered, counting for the M_w standard deviation, too (Eq [17]). The corresponding maximum error of the average M_w is 0.0164.

The total maximum "artificial" M_w error based on the combination of the correspondings maximum errors of the three above scaling factors can reach the ~ 0.173 ($0.0446+0.1116+0.0164$), lower than the common ~ 0.2 estimated standard deviation of moment magnitudes and local magnitudes.

Regarding the initially unknown Mean Free Path, l (MFP), controlling the excitation factor, E_c (Eq. [4, 5]), although it can significantly differ at different tectonic statement, it can be considered equal to the mean free path at isotropic scattering conditions. The corresponding typical MFP values at these conditions are mainly range between 10 to 1000 km, according to measured values from several studies (*Sato, 1978, Margerin et al. 1999, Lacombe et al. 2003*). This range can be considered as the standard deviation range with a geometric mean value of 100 km, for the STF and M_o computation strategy. However, based on these values the corresponding maximum M_w error (Eq. [16]) is quite significant (~ 0.333).

Thus, in case that the second computation strategy is chosen for the STF scaling M_o estimation, the total ~ 0.5 ($0.173 + 0.333$) standard deviation of the moment magnitude must be considered, independently of the standard deviation range that has been computed for the unscaled STF and M_o .

Taking into account this initially input 0.5 standard deviation it is obvious that the seismic moment and the real STF amplitude cannot be precisely estimate when MFP is unknown. This is confirmed from **Figure 10**, moment magnitudes, M_w are computed based on the second STF and M_o scaling strategy, for three different mean free paths: 10, 100, 300 km and they are compared to the local magnitudes, ML determined by the Seismological Station of A.U.Th. (<http://geophysics.geo.auth.gr/ss/>). It is obvious that their scaling is mainly controlled by the MFP and not by the rest total standard deviation, controlled by the ρ , β , v_s scaling factors (Eq. [9, 16]) and by the propagated STF standard deviation (e.g. **Figure 9d**). From **Figure 10** it can be also observed that the moment magnitudes, $M_{w_{STF}}$ computed at least for one the three different MFPs, lie on the typical standard deviation range of the local Magnitude (0.2). This observation confirms that the MFP values ranges around 10-1000km, supporting the valid application of the STF methodology as proposed by *Sebe et al. 2018* and partially revised in this study.

What is also observed from **Figure 10** is the relevant variability of the MFP between the different sites but also between the different earthquakes at each site. Trying to have a better understanding of this variability, the mean free paths were inversely computed (**Figure 11**) for each pair of earthquake–station studied here (**Figure 1a**), based on the local magnitudes by the following process. Initially the seismic moment M_o , of each earthquake was computed based on Eq. [15], considering moment magnitude, M_w equal to the already known local magnitude, ML from the Seismological Station catalogue of A.U.Th. (<http://geophysics.geo.auth.gr/ss/>). The $ML = M_w$

assumption is not absolutely true, but it can give as a first view of the mean free path variability taking into account the ML standard deviation (~ 0.2) but also the “artificial” (~ 0.173) standard deviation computed for ρ , β , ν (Eq. [17]), mentioned above at this sub-chapter. No clear correlation is presented in **Figure11** between MFP and azimuth-epicentral distance of each earthquake STF estimated at each site.

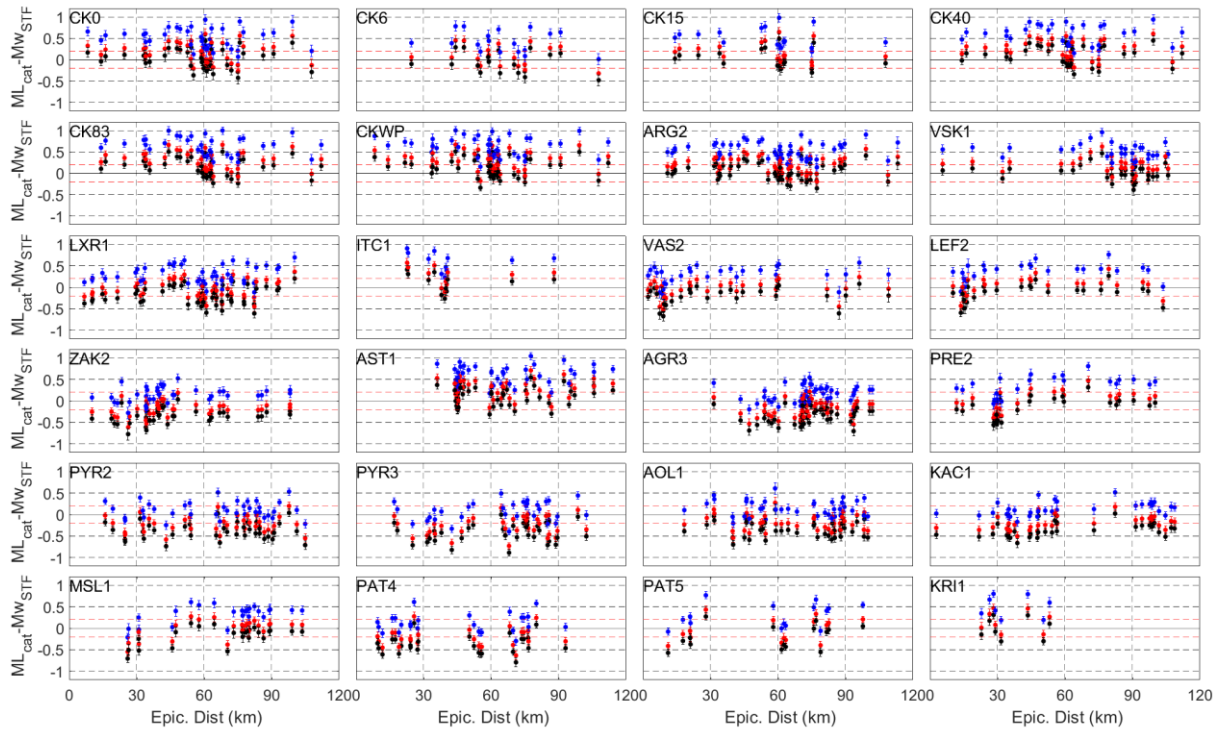


Figure 10. The difference between the local magnitude ML_{cat} from catalogue (<http://geophysics.geo.auth.gr/ss/>) and the computed moment magnitude, M_{wSTF} based on the 2nd computation strategy (information to the: “STF” scaling and M_o computation” sub-chapter) for three difference mean free paths: 10, 100, 300 km (blue, red, black points).

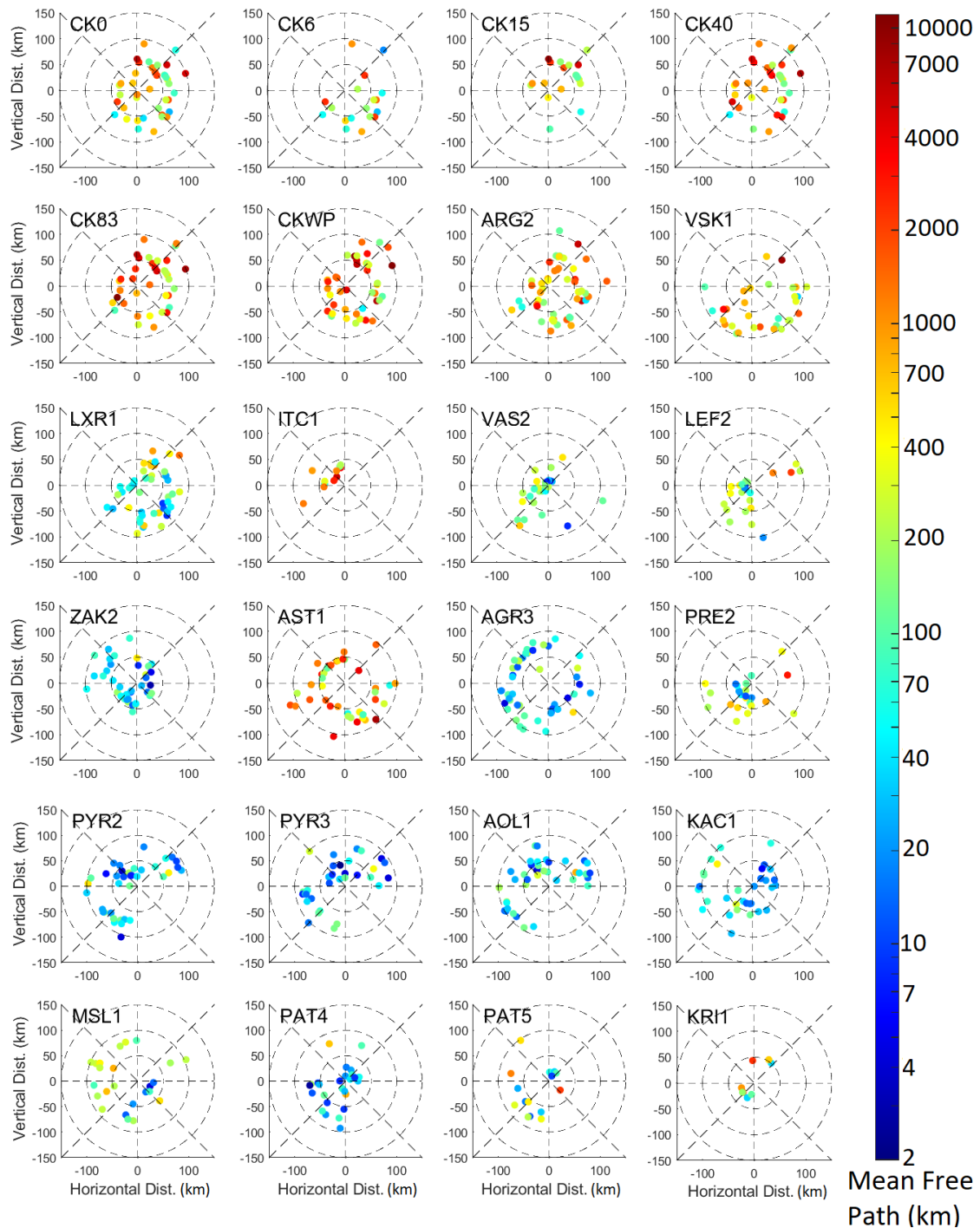


Figure 11. The Mean Free Path (km) estimated from each earthquake at each station of the 24 (Figure 1a). The center of each sub-figure (0,0 position) is the position of the station. Dashed cycles correspond to 50, 100 and 150 km radius.

4 Site effect Estimation

The minimum phase STF (in displacement) computed from the “unscaled estimated STF process at a reference site”, mentioned above, is considered as the real STF (*Sebe et al. 2018*) unscaled for frequency independent factor \sqrt{F} (Eq. [9, 12]), only in case where the low frequency plateau can be observed so that the STF

to be corrected (**Figure 8d,9b**). At this case (reference site) the non-amplification at low frequencies hypothesis is quite reasonable and the low frequency correction, if possible, tends to be a quite reliable process.

The same non-amplification at low frequencies hypothesis for the non-reference site can be also assumed so that the unscaled STF being corrected for the plateau. However, it is worth noting that at this case the presented low frequency plateau could be ostensible, due to a stable amplification at the low examined frequencies. Therefore, the STF low frequency correction, at non-reference sites, could not be reliable and the corrected STF could not be valid. This hypothesis is actually under investigation at this study and the reliable expected TF(f) for these sites, if they will be estimated, are going to support the potential of the technique to retrieve the reliable STF at these site after a valid low frequency plateau correction, or not.

However, at any case (reference or not) the unscaled STF FAS at the reliable (form SNR process) frequency part, remains valid and independent of the STF(t) detection after the correction of the low frequency plateau.

Regarding the Site Spectral Amplification (so-called Transfer Function, TF) computation, which is the main goal of the proposed technique, it is reasonable considering that the ratio of the Fourier Amplitude Spectra ($FAS(f)$) of the scaled STF(f) (site effect included) computed from the same earthquake at two different site, from which the one is a reference site ($TF_{ref}(f) = 1$), can reveal the TF_{targ} at the other site (“target”). This is relation is expressed in Eq. [18], where the FAS(f) of the scaled STF(t) (site effect included) is simply considered as the product of the FAS(f) of the real STF(t) with the TF(f) of the site, according to fundamental Eq. [1]).

$$\frac{FAS(f)_{targ}}{FAS(f)_{ref}} = \frac{TF(f)_{targ}}{TF(f)_{ref}} \Leftrightarrow \frac{FAS(f)_{STF} \cdot TF(f)_{targ}}{FAS(f)_{STF} \cdot TF(f)_{ref}} = \frac{TF(f)_{targ}}{TF(f)_{ref}} = TF(f)_{targ} \quad [18]$$

This technique is similar to the Standard Spectra Ration technique (**Borcherdt, 1970**), where the FAS(f) ratio of the body S-wave, between a target and a reference station can reasonably approach the $TF(f)_{targ}$, but without the condition of the adjacent station, securing the similar ray paths. At the case expressed by Eq. [18], and assuming isotropic soured energy radiation, the $TF(f)_{targ}$ can be determined independently of the distance between the station. However, the STFs(f) computed in this study are unscaled for the factor unknown factor \sqrt{F} (Eq. [9, 12]), and the same for their FAS(f), where:

$$FAS(f) = FAS(f)_{unsc} / \sqrt{F} \quad [19]$$

Thus, according to Eq. [19] and [9], the Eq. [18] can be written as:

$$\begin{aligned} TF(f)_{targ} &= \frac{FAS(f)_{targ}}{FAS(f)_{ref}} = \frac{FAS(f)_{unsc_{targ}} / \sqrt{F_{targ}}}{FAS(f)_{unsc_{ref}} / \sqrt{F_{ref}}} = \\ &= \frac{FAS(f)_{unsc_{targ}} \cdot v_{starg} \sqrt{\pi^2 \rho \beta^5 l_{targ}}}{FAS(f)_{unsc_{targ}} \cdot v_{ref} \sqrt{\pi^2 \rho \beta^5 l_{ref}}} = \frac{FAS(f)_{unsc_{targ}} \cdot v_{starg} \sqrt{l_{targ}}}{FAS(f)_{unsc_{targ}} \cdot v_{ref} \sqrt{l_{ref}}} \end{aligned} \quad [20]$$

Based on Eq. [20] three simple conclusions can be extracted:

- 1) The ratio of the unscaled FAS(f) at the two sites (target and reference) can reveal the TF(f) of the target site, only under the condition that the two scaling factors F (F_{targ} and F_{ref}), are known, or\and are unknown but similar. The last means that the average shear wave velocity v_s corresponding to the coda waves path from the earthquake to the target and reference site (v_{starg} and v_{sref}), as well as the corresponding mean free paths, l (l_{targ} and l_{ref}), must be similar, so that the TF(f) being reliable.
- 2) Taking into account the reasonable standard deviation range of the v_s and l parameters (3-4 km/sec and 10-300 km, respectively), the maximum difference between the computed TFs(t) at target site from several earthquake can reach up to ~ 7 times (lower or higher) between each other. This measurement is defined following the same strategy as at the “*STF scaling and M_o computation*” mentioned above, but based on the $v_s \cdot \sqrt{l}$ ration between the target and the reference site (Eq. [20]), for their reasonable standard deviation range values.

3) Although the real $TF(f)_{\text{targ}}$ amplitudes of the target site depends on the constant values, v_s and l , the relevant $TF(f)_{\text{targ}}$ amplification between the examined frequencies are independent of these values and can be theoretically revealed after applying the technique expressed by Eq. [20].

Below, the horizontal component $TF(f)$ of the 24 stations examined in this study (**Figure1, Appendix A**), are computed in comparison to four reference sites, applying the proposed technique expressed by Eq. [20], without the knowledge of the shear wave velocity, v_s and mean free path, l . The $TF(f)$ estimation were achieved after computing the unscaled $STF(t)$ (Eq. [12]), of the 89 earthquakes, also examined here (**Figure 1, Appendix B**), at these sites, where it was feasible, only for the horizontal components (Eq. [13]). This application aims to two achieve to goals.

1) To confirm the second and the third conclusions only by the stability of the $TFs(f)$ “shape” and by the maximum ~ 7 times difference between the $TF(f)$ at each site.

2) To investigate the similar v_s and l hypothesis as a function of the reference to target site distance, after detecting the stable $TFs(f)$ at each site, if possible and comparing them to the computed $TF(f)$ derived from other methods.

More specifically the horizontal component $TF(f)$ of the 5 “CK..” (CK0, CK6, CK15, CK40, CK83) stations (**Appendix A**), have been also computed from SSR technique applied in this study, in comparison to the nearby (~ 0.4 km) rock installed “CKWP” station. Body S-waves records, necessary for the SSR application, of the horizontal components, of the dataset used for the STF computation, was chosen based on the strategy proposed by *Perron et al 2018*. Stress drop, $\Delta\sigma = 10$ bar, duration equal to $0.1 \cdot R_{\text{hyp}}$ (R_{hyp} hypocentral distance, in km), Signal to Noise Ratio (f) greater than 5 and minimum reliable FAS(f) corresponding to a minimum of eight signal cycles are the criterion for the S-wave record selection. The Fourier Amplitudes Noise spectra was chosen the one already computed for the STF estimation methodology mentioned above at this study (e.g. **Figure 3**). The results of this SSR application for the “CK0” station are identical to the one computed by *Hollender et al. 2018*.

Before the computation of the horizontal components $TF(f)$ and their comparison to the corresponding one based on the SSR technique of S-waves, the theoretically potential of their right comparison should be firstly investigated. This must be achieved, because the application of the proposed $TF(f)$ estimation technique refers to the maintenance of energy of the same seismic source at two difference site and its right implementation should be taking into account all the three components (Eq. [13]) and not only the Horizontal one. However, approving that the Horizontal to Vertical Spectral Ratio (HVSR) of the computed STF FAS is identical to the corresponding one computed by the direct body S-waves (also computed for the same dataset), the maintenance of the energy distribution will be the same between Horizontal and Vertical components for the direct and coda S-waves and the comparison between the $TFs(f)$ computed from SSR and from the proposed technique will be theoretically valid. In **Figure 12** the above consideration is confirmed, since the computed HVSR of the direct body S- wave FAS and of the STF FAS are identical.

Moreover, the $TF(f)$ of the rest 18 ITSAK station-sites (Appendix A) estimated by *Grendas et al. 2018* applying a Generalized Invasion Technique (GIT), are compared to the $TF(f)$ computed by the technique proposed in this study. It is worth noting that the SSR $TFs(f)$ of the 5 “CK..” sites constitute absolute reliable amplifications values that is to be compared to the corresponding $TFs(f)$ resulting from the proposed technique, while the computed $TFs(f)$ from the GIT are not at the same reliability level, since they are built under several assumptions, like the common attenuation model for a large area, or the uncertainties of the Seismic Source function and they are not been confirmed by other methods. However, it is reasonable to consider that these results tend at least to approach the real average $TF(f)$ of each site.

The last goal (2) mentioned above, is going to experimentally defining the applicability potential of the proposed technique, regarding the maximum distance of a reference station, based on real data.

The stations used as reference in the $TF(f)$ computation at all the examined sites, are the: “CKWP”, “ITC1”, “VSK1” and ‘AST1”. These stations are installed on surface rock sites and their spectral amplification is expected being equal to one (no amplification) for each frequency. The minimum distance between these reference stations is ~ 15 km and the maximum ~ 65 km (**Figure 1a**). The distances between the target and reference sites range between 0.4 km to ~ 110 km.

In **Figure 12**, the TF(f) of the 23 stations (**Figure 1**) were computed in comparison to the “CKWP” reference station, based on the unscaled STF FAS.

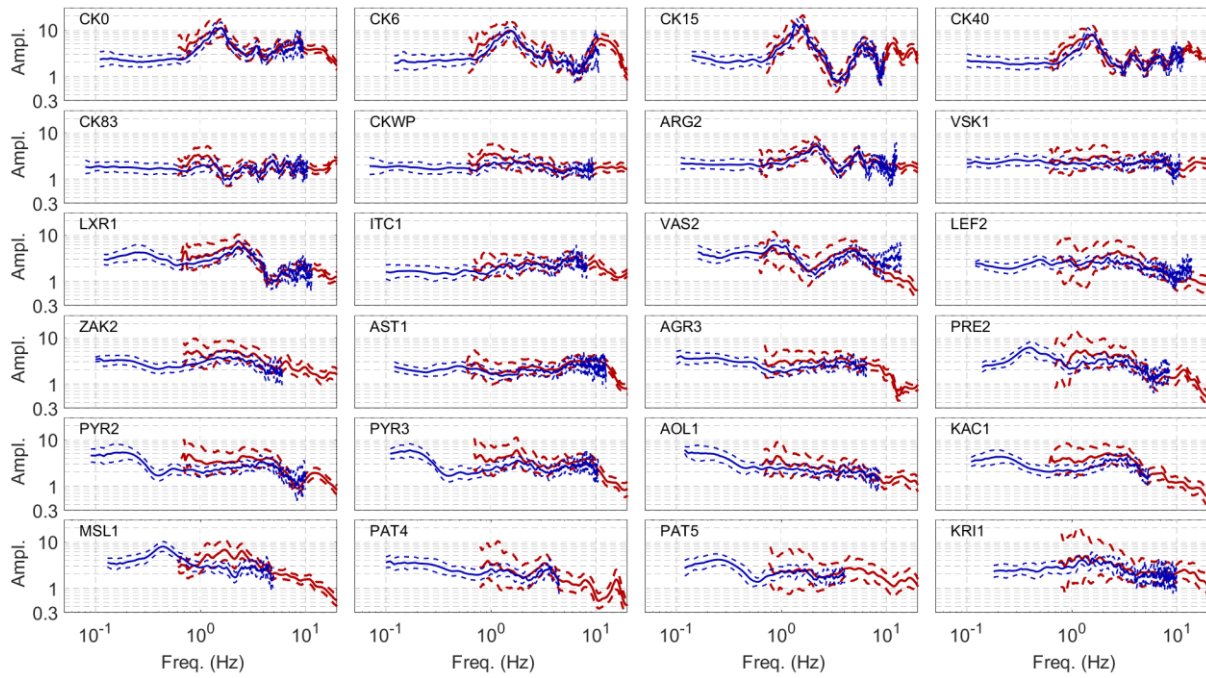


Figure 12. The HVSRs (red and blue lines), computed from the direct S-wave (details into the current sub-chapter) and from the calculated STFs in this study.

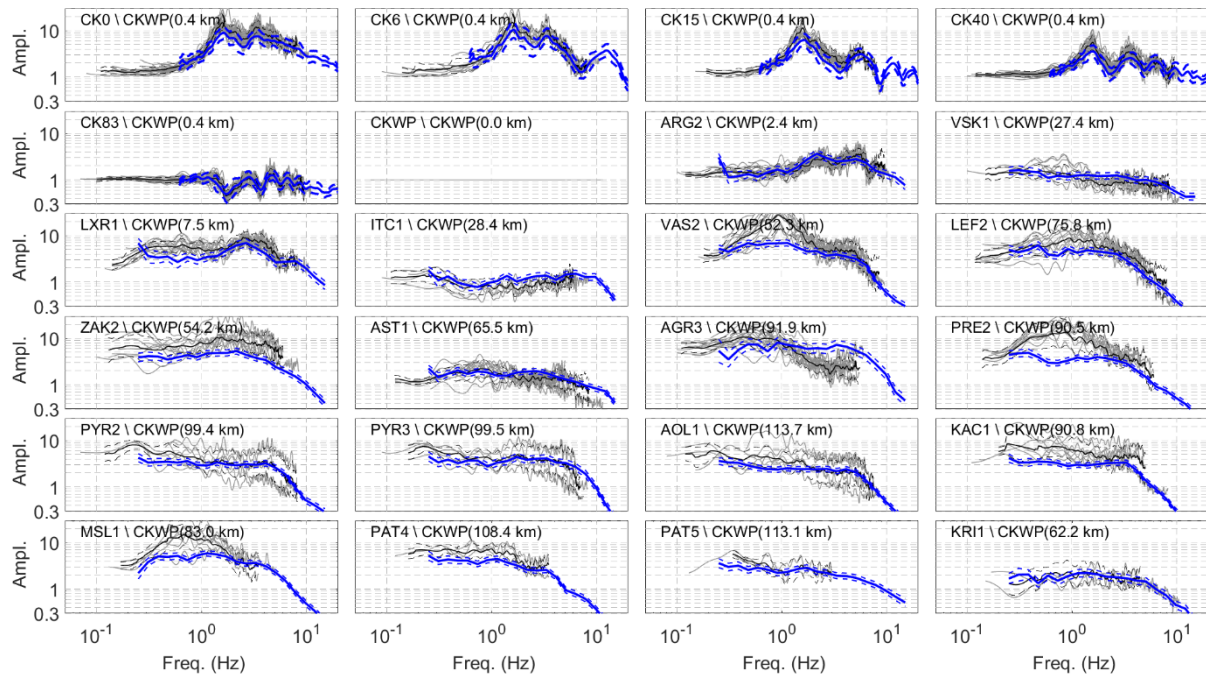


Figure 13. The TFs(f) of each one of the 24 examined sites (**Figure 1**) as computed by: 1) the proposed technique based on STF (grey lines-black line the average) using the “CKWP” as reference station. 2) the SSR technique (blue lines) for the 5 CK.. stations and 3) by the GIT (*Grendas et al. 2018*) method for the rest 18 ITSAK stations (blue lines).

The relevant stability of the TFs(f) shape for each site and their maximum difference which is below 7 times between each other, confirms the first goal of the proposed technique, mentioned direct above. Regarding the second goal of the similar average shear wave velocity and mean free path that is expected to conclude at similar TF(f) absolute amplitudes between the computed from the proposed technique (grey lines), it seems that is confirmed mainly when reference-target site distance is lower than ~30 km. This is based on the TFs(f) (grey lines) computed for the: “CK.. (5 sites)”, ARG2, VSK1, LXR1, ITC1, taking into account the TF(f) scattering around their geometrical mean (black line) for each site. Moreover, what is also support the valid applicability of the proposed technique is the quite good agreement (under their statistical error expressed by their standard deviation range) between the absolute TF(f) amplitudes of the geometrical means (black lines) for these 9 sites and the corresponding TFs(f) determined from SSR and GIT method (blue lines), for the “CK.. (5 sites)” and the rest 4 ITSAK stations, respectively.

It is worth noting the geometric mean of the 5 “CK..” sites computed by the proposed technique (black lines), indicated a bit overestimation (less that a factor of 2) in comparison to the corresponding TF(f) computed by SSR for the same reference station: “CKWP”. However, they statistically agree, since their standard deviation ranges are ~ 50% overlapped. This overlap much to the fact that the TF(f) computed by the proposed technique refereeing to coda waves, corresponds to the upper standard deviation range values of the SSR based on the S-waves. This observation is identical to the one presented by *Margheriti et al. 1994* supporting that “*the coda amplifications generally yields upper bounds for the S-wave amplifications on the frequency band (0.5 to 10 Hz)*”.

The same TFs(f) results were computed using as reference the: “VSK1”, “ITC1”, and “AST1”, rock installed station and presented in **Figure 14, 15** and **16** respectively. However, at these three sites the absolute TF(f) amplification estimated by *Grendas et al. 2018*, seem to differ from values exactly equal to one (reference). For this reason the computed geometric mean (black lines) of the TFs(t) estimated by STFs for all ITSAK sites (ARG2, VSK1, LXR1, ITC1, VAS2, LEF2, ZAK2, AST1, AGR3, PRE2, PYR2, PYR3, AOL1, KAC1, MSL1, PAT4, PAT5 and KRI1), were corrected (red lines) for the absolute TF(f) (blue lines) of the three sites considered as reference, respectively, so that being right-comparable to their corresponding TF(f) (blue lines). Moreover, the computed geometric mean (black lines) of the TFs(t) estimated by STFs for the ARGOnet sites (CK0, CK6, CK15, CK40, CK83 and CKWP) were corrected (red lines) based on the TF(f) of the CKWP, (used as reference at the SSR method), so that the results being also right-comparable to the SSR ones. The corrections for the first case expressed by the multiplication of the black lines to the blue line of each reference site at each case of **Figure 14, 15** and **16**, respectively, while at the second case they achieved by dividing the computed black lines of the 5 “CK..” sites to the computed black line of the “CKWP”.

From the corrected TFs(f) results (red lines) of **Figure 14, 15** and **16**, based on three distant between each other reference station, the first goal of the proposed technique that mentioned above is achieved, too. Regarding the second goal, it also seems that at reference-target site distances up to ~30 km the applicability of the method is quite valid in detecting the absolute TF(f) amplifications under their computed standard deviation range.

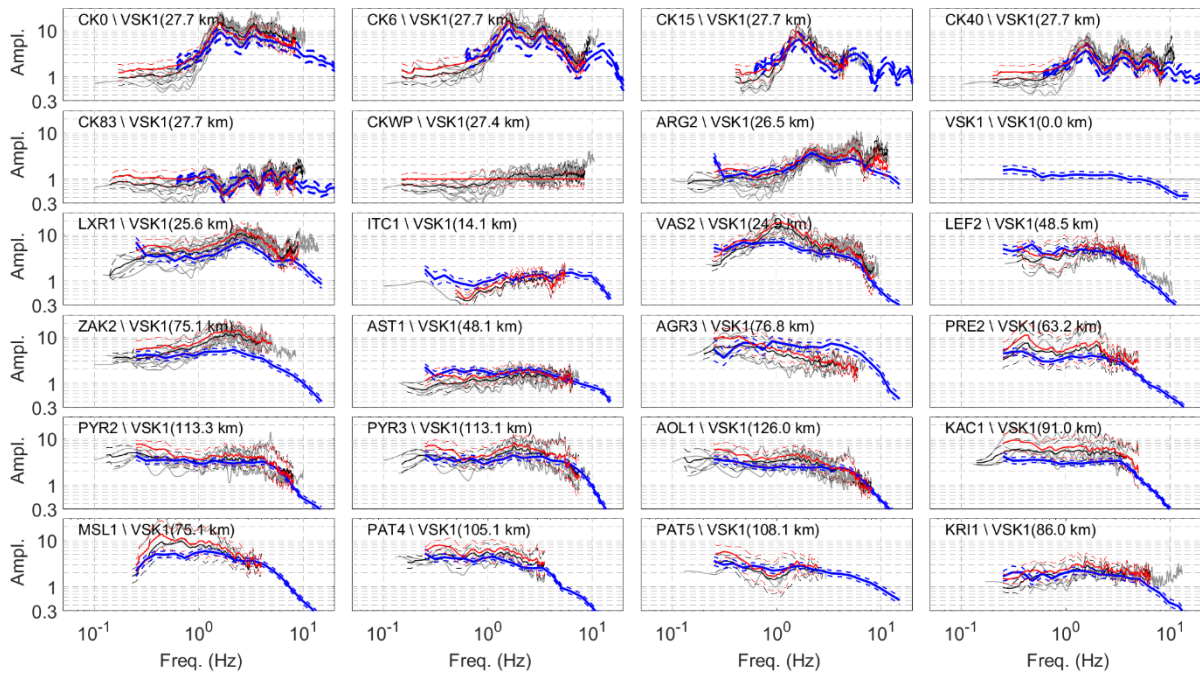


Figure 14. The corresponding to Figure 13, TFs(f) using the “VSK1” as reference (black lines). The corrected black lines (red lines) (information above into the manuscript at the current chapter) and the distance between target and reference site are also presented.

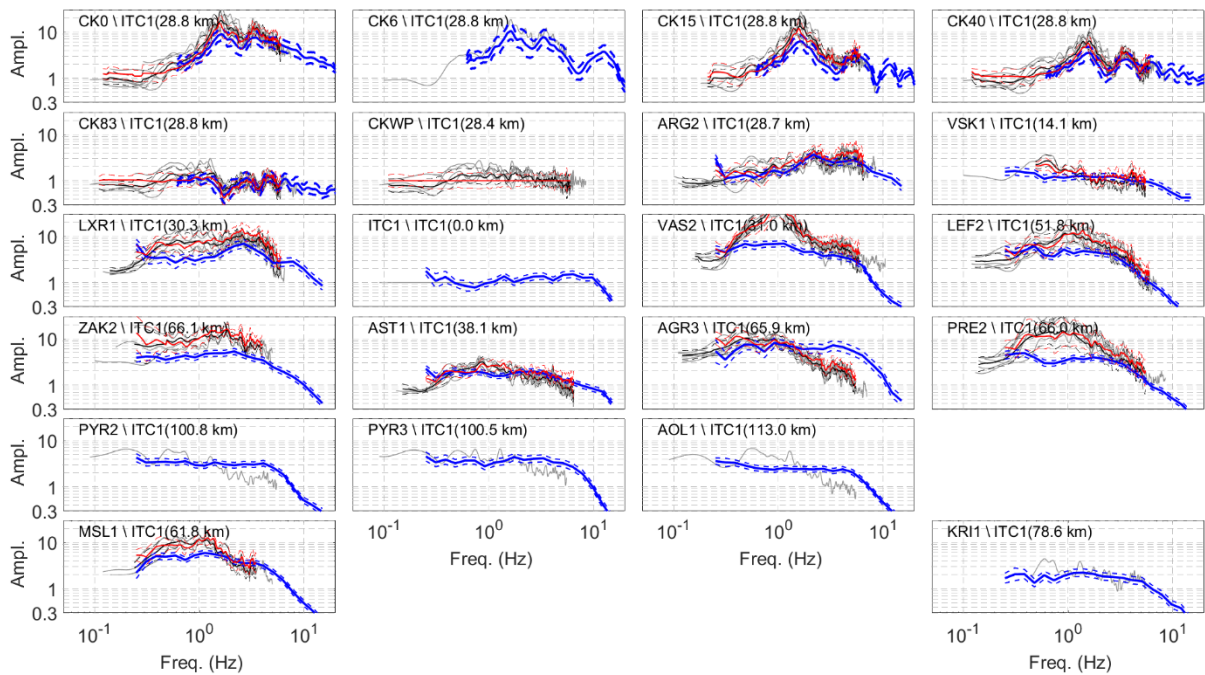


Figure 15. The corresponding to Figure 13, TFs(f) using the “ITC1” as reference (black lines). The corrected black lines (red lines) are also presented (information above into the manuscript at the current chapter). Empty figures “belong” to the corresponding sites of Figure 14, for which no TF from STF were computed.

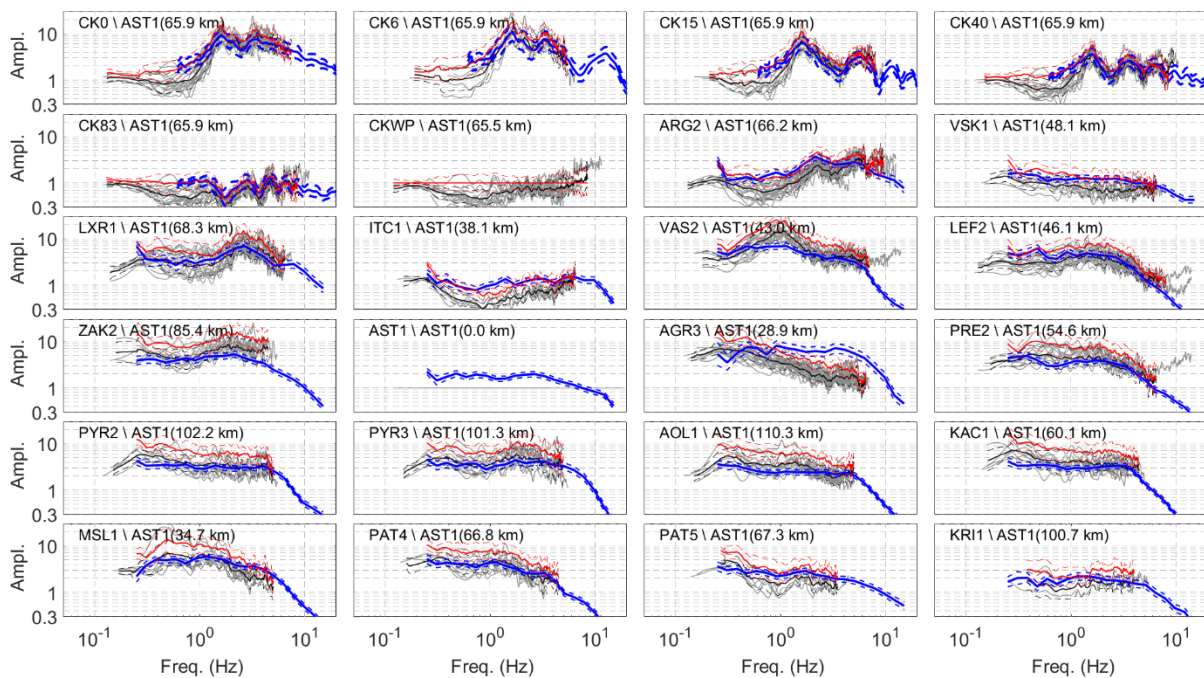


Figure 16. The corresponding to Figure 14 ,15, TFs(f) using the “AST1” as reference (black lines). The corrected black lines (red lines) are also presented (information above into the manuscript at the current chapter).

Discussion – Conclusions

A new Transfer Function (TF) estimation technique, using real earthquake data (coda wave records), is presented and examined in this study. Based on the comparison between the unscaled STF as computed at a target and a reference (rock site), a process similar to the commonly used one Standard Spectral Ratio (*Borcherdt, 1970*), is applied, revealing the TF. The estimated STFs are unscaled by the constant excitation factor, E_c and the average shear wave velocity, v_s on the crust, and the valid application of the proposed TF estimation technique depend on the precondition of the similar scaling factors of v_s and E_c . Based on the results of the study, this precondition seems to be true at least for ~ 30 km distance between reference and target stations is.

The STF computation is achieved by a multiple step methodology, proposed by *Sebe et al. 2018* and which is applied on single station velocity coda wave records (3-components). The methodology algorithm used in this study is a re-developed (free to use) MATLAB one, based on the one developed by *Sebe et al. 2018*, but using several alternative processes.

A quite strict and easy to be managed by the user, Signal to Noise Ratio (SNR) process-algorithm, was developed and is initially applied in order to detect the best choice of coda time window in relation to the examined frequency range. Thereupon, a time decay rate analysis of coda wave envelopes for 20 central frequencies, is applied at each component, separately, and the common frequency dependent coda quality factors, $Q_c(f_{cen})$ and their standard deviation, are computed. Based on these $Q_c(f_{cen})$ values, the $Q_c(f)$ model that express better the $Q_c(f_{cen})$, following the single scattering model (*Aki and Chouet, 1975*), and its standard deviations, are estimated. This model and its one standard deviation range values are used for the attenuation factor removal from the coda wave record.

Three different corrected – stationary coda wave records are retrieved for each pair of earthquake-station. By this strategy, the attenuation model uncertainty is taken into account at the final STF computation, trying to give the reliability level of the computed STF, as possible. Thereafter, from the autocorrelation of these stationary coda waveforms, the unscaled, for the constant scaling factors (Eq. [9]), velocity STF Fourier Spectra (FS), (Site amplification included) is detected, following the suitable process mentioned above into the study. By the use of “rceps” Matlab function the minimum phase of these velocity STFs, at each component is computed. Based on the geometrical contribution of the STF horizontal components the corresponding FAS spectra are computed.

Regarding the TF estimation strategy, the computed horizontal STF FAS of an earthquake at two station from which the one is considered as reference, are compared between each other, revealing the target station TF. The TF of 24 site in western Greece (**Figure 1**), in comparison to four distant between each other (from ~15 to ~65 km) reference considered (rock) sites (CKWP, ITC1, VSK1 and AST1), were computed, following the suitable analysis steps of the proposed technique (**Figure 2**). Based on this analysis steps, it is worth noting that the TF estimation can be achieved also at step 8, by the use of the velocity unscaled STF and not necessarily at step 11 (**Figure 2**), at the displacement corresponding ones.

More than 700 STFs of 89 earthquakes in this high seismicity area, were used for the application of the proposed TF estimation technique. The results of the computed TF at the 24 examined sites (**Figure 13, 14, 15 and 16**) supports the theoretical expected corresponding results, referring to the first goal of the application for which the stability between the TFs(f) “shape” of each station and the maximum ~ 7 times difference between them must be presented. Moreover, the results partially confirm the valid applicability of the proposed TF estimation technique under the assumption of the similar the constant excitation factor, E_c and the average shear wave velocity, v_s on the crust. It seems that for reference – target site distances lower than ~30 km, this assumption is true, where the estimated TFs of the target site are generally stable and their geometric mean is identical to the corresponding SSR (**Bocherdt, 1970**) TF.

The estimated average TF from the proposed technique seems to “lie on” the upper standard deviation limit of the corresponding SSR one for the non-reference site (e.g. CK0 at **Figure 13, 14, 15 and 16**), in agreement to the same observation by **Margheriti et al. 1994**, comparing SSR TF based on direct shear and coda wave. However, for sites of non-high amplifications, the computed TF results of the proposed technique seems being identical to the corresponding SSR ones (e.g. CK83 at **Figure 13, 14, 15 and 16**) following **Margheriti et al. 1994**, too.

It is important to mention that the applicability of the proposed TF estimation technique is based on the hypothesis of the isotropic source energy radiation. This seems to be true for the earthquakes examined in this study (ML = 3.9-5.1) and it is confirmed by the similar “shape” between the computed TFs. Probably the seismic sources of these non-high magnitude earthquakes, may approach a simple pulse wavelet.

Some extra observations are also revealed by the present study. 1) Regarding the quality factor, $Q_c(f)$ modeling, it is confirmed that Eq. [7] can express it only for frequencies greater than ~1 Hz, while the for lower frequencies the $Q_c(f)$ values can be increased. 2) The uncertainty comes from the unknown excitation factor can reach the relevant significant ~0.33 magnitude error, while the corresponding magnitude error by the rest scaling factors Eq. [9], is up to ~0.17. 3) The low frequency plateau that is detected at non-reference, indicating the stable no-amplification at low frequencies can be ostensible. This is confirmed by the estimated TF at the CK0 and LXR1, non reference sites, where at the first one no amplification at the low frequencies is confirmed, while at the second one stable amplification up to 3-4 times, contaminates the low frequency STF plateau, without being obvious. 4) In case that the low frequency STF FAS plateau is detected and it is valid (mainly at reference stations, based on the above observation) and using the “STF scaling and M_o computation” strategy analyzed at the corresponding sub-chapter, the expected magnitude error is ~0.5, independent on the standard deviation range computed from the unscaled STF.

References

- Aki, K., 1969. Analysis of the seismic coda of local earthquakes as scattered waves. *Journal of geophysical research*, 74(2), pp.615-631.
- Aki, K. and Chouet, B., 1975. Origin of coda waves: source, attenuation, and scattering effects. *Journal of geophysical research*, 80(23), pp.3322-3342.
- Aki, K., 1980a. Scattering and attenuation of shear waves in the lithosphere. *Journal of Geophysical Research: Solid Earth*, 85(B11), pp.6496-6504.
- Aki, K., 1980b. Attenuation of shear-waves in the lithosphere for frequencies from 0.05 to 25 Hz. *Physics of the Earth and Planetary Interiors*, 21(1), pp.50-60.
- Borcherdt, R. D. (1970). Effects of local geology on ground motion near San Francisco Bay, Bull. Seismol. Soc. Am. 60, 29–61.
- Dainty, A.M., 1981. A scattering model to explain seismic Q observations in the lithosphere between 1 and 30 Hz. *Geophysical Research Letters*, 8(11), pp.1126-1128.

- Dolan, S. S., C. J. Bean, and B. Riollot (1998). The broad-band fractal nature of heterogeneity in the upper crust from petrophysical logs, *Geophys. J. Int.* 132, 489–507.
- Grendas, I., Theodoulidis, N., Hatzidimitriou, P., Margaris, B. and Drouet, S., 2018. Determination of source, path and site parameters based on non-linear inversion of accelerometric data in Greece. *Bulletin of Earthquake Engineering*, 16(11), pp.5061-5094.
- Gusev, A. A., and I. R. Abubakirov (1996). Simulated envelopes of non-istropically scattered body waves as compared to observed ones: nother manifestation of fractal heterogeneity, *Geophys. J. Int.* 127, 49–60.
- Hanks, T., C. and Kanamori, H., (1979). A moment magnitude scale, *J. Geophys. Res.* 84, no. B5, 2348/2350.
- Hatzidimitriou, P.M., 1993. Attenuation of coda waves in Northern Greece. *pure and applied geophysics*, 140(1), pp.63-78.
- Herraiz, M. and Espinosa, A.F., 1986. *Scattering and attenuation of high-frequency seismic waves; development of the theory of coda waves* (No. 86-455). US Geological Survey.
- Hollender, F., Roumelioti, Z., Régnier, J., Perron, V. and Bard, P.Y., 2018. Respective advantages of surface and downhole reference stations for site effect studies: lessons learnt from the ARGONET (Cephalonia Island, Greece) and Cadarache (Provence, France) vertical arrays. In *Proceedings of the 16th European Conference on Earthquake Engineering (16ECEE), Thessaloniki, Greece*.
- Lacombe, C., M. Campillo, A. Paul, and L. Margerin (2003). Separation of intrinsic absorption and scattering attenuation from Lg coda decay in central France using acoustic radiative transfer theory, *Geophys. J. Int.* 154, 417–425.
- Margerin, L., Campillo, M. and Tiggelen, B., 1998. Radiative transfer and diffusion of waves in a layered medium: new insight into coda Q. *Geophysical journal international*, 134(2), pp.596-612.
- Margerin, L., Campillo, M., Shapiro, N.M. and van Tiggelen, B., 1999. Residence time of diffuse waves in the crust as a physical interpretation of coda Q: application to seismograms recorded in Mexico. *Geophysical Journal International*, 138(2), pp.343-352.
- Margheriti, L., Wennerberg, L. and Boatwright, J., 1994. A comparison of coda and S-wave spectral ratios as estimates of site response in the southern San Francisco Bay area. *Bulletin of the Seismological Society of America*, 84(6), pp.1815-1830.
- Perron, V., Laurendeau, A., Hollender, F., Bard, P.Y., Gélis, C., Traversa, P. and Drouet, S., 2018. Selecting time windows of seismic phases and noise for engineering seismology applications: A versatile methodology and algorithm. *Bulletin of Earthquake Engineering*, 16(6), pp.2211-2225.
- Rautian, T.G. and Khalturin, V.I., 1978. The use of the coda for determination of the earthquake source spectrum. *Bulletin of the Seismological Society of America*, 68(4), pp.923-948.
- Sato, H. 1977. Energy propagation including scattering effects sengle isotropic scattering approximation. *Journal of Physics of the Earth*, 25(1), 27-41.
- Sato, H., 1978. Mean free path of S-waves under the Kanto district of Japan. *Journal of Physics of the Earth*, 26(2), pp.185-198.
- Sato, H., 1982. Attenuation of S waves in the lithosphere due to scattering by its random velocity structure. *Journal of Geophysical Research: Solid Earth*, 87(B9), pp.7779-7785.
- Sato, H., Fehler, M. C., & Maeda, T. (2012). *Seismic wave propagation and scattering in the heterogeneous earth*. Springer Science & Business Media.
- Sèbe, O., Guilbert, J. and Bard, P.Y., 2018. Spectral Factorization of the Source Time Function of an Earthquake from Coda Waves, Application to the 2003 Rambervillers, France, Earthquake. *Bulletin of the Seismological Society of America*, 108(5A), pp.2521-2542.
- Singh, S. and Herrmann, R.B., 1983. Regionalization of crustal coda Q in the continental United States. *Journal of Geophysical Research: Solid Earth*, 88(B1), pp.527-538.
- Soham, B. and Abhishek, K., 2016. Determination of seismic wave attenuation: A Review. *A A*, 2(1), p.1.
- Theodoulidis, N., Hollender, F., Mariscal, A., Moiriat, D., Bard, P.Y., Konidakis, A., Cushing, M., Konstantinidou, K. and Roumelioti, Z., 2018. The ARGONET (Greece) seismic observatory: An accelerometric vertical array and its data. *Seismological Research Letters*, 89(4), pp.1555-1565.
- Tselentis, G., 1998. Intrinsic and scattering seismic attenuation in W. Greece. *pure and applied geophysics*, 153(2-4), pp.703-712.
- Vassiliou, M.S. and Kanamori, H., 1982. The energy release in earthquakes. *Bulletin of the Seismological Society of America*, 72(2), pp.371-387.

Appendix A

Table A.1. The coordinates of the 24 stations, the records of which are used at this study. The symbols: “I” and “A” indicate the stations that belong to the ITSAK (<http://www.itsak.gr>) and to the ARGOnet (<http://argonet-kefalonia.org/>) accelerometric networks.

	Station	Latitude (°)	Longitude (°)	Network		Station	Latitude (°)	Longitude (°)	Network
1	CK0	20.506248	38.164152	A	13	ZAK2	20.8999	37.7878	I
2	CK6	20.506248	38.164152	A	14	AST1	21.0895	38.5416	I
3	CK15	20.506248	38.164152	A	15	AGR3	21.4161	38.5892	I
4	CK40	20.506248	38.164152	A	16	PRE2	20.7546	38.9576	I
5	CK83	20.506248	38.164152	A	17	PYR2	21.4505	37.6671	I
6	CKWP	20.510489	38.166288	A	18	PYR3	21.4623	37.6787	I
7	ARG2	20.4877	38.1783	I	19	AOL1	21.6247	37.6433	I
8	VSK1	20.564	38.409	I	20	KAC1	21.5481	38.1379	I
9	LXR1	20.4374	38.2009	I	21	MSL1	21.4243	38.3726	I
10	ITC1	20.7155	38.3645	I	22	PAT4	21.7478	38.2341	I
11	VAS2	20.6081	38.6303	I	23	PAT5	21.795	38.2959	I
12	LEF2	20.7081	38.8302	I	24	KRI1	20.817185	37.662063	I

Appendix B

Table B.1. The information (Id. Coordinated and local magnitude, ML) of the 89 earthquakes, the records of which used in this study. ML are referred to the catalogue published by the Seismological Station of Aristotle University of Thessaloniki (<http://geophysics.geo.auth.gr/ss/>).

	Eaerthquake id (Year-Month- Day_time)	Lat. (°)	Long. (°)	ML		Eaerthquake id (Year-Month- Day_time)	Lat. (°)	Long. (°)	ML
1	20151023_171318	20.193	37.990	3.9	46	20171104_095115	21.420	37.840	4.1
2	20151117_083340	20.557	38.651	5.1	47	20171214_020835	19.800	37.640	4
3	20151117_114945	20.485	38.486	4.1	48	20171225_234705	20.560	38.590	4.4
4	20151117_115725	20.614	38.702	4.4	49	20180221_234455	20.350	37.790	4.8
5	20151117_123756	20.653	38.702	4.5	50	20180222_070750	21.620	38.130	3.9
6	20151117_193934	20.601	38.704	4.5	51	20180424_052345	21.780	38.210	3.8
7	20151118_051813	20.517	38.496	4.5	52	20180705_213905	21.290	37.960	4.4
8	20151118_121538	20.591	38.844	4.9	53	20180714_050846	21.820	37.700	3.8
9	20151118_130314	20.628	38.719	4.6	54	20180818_032649	21.820	38.380	3.8
10	20151118_183007	20.628	38.723	4.1	55	20180831_071224	21.630	39.290	5

11	20151119_174555	20.495	38.462	4	56	20180831_082623	21.610	39.350	4.1
12	20151120_051224	20.487	38.470	4.8	57	20180918_024843	21.570	38.120	4
13	20151120_093314	20.583	38.634	4.6	58	20181027_052846	20.640	37.470	4.6
14	20151120_233704	20.617	38.710	4.4	59	20181030_025959	20.510	37.590	5.4
15	20151121_004156	20.617	38.714	4.6	60	20181105_064613	20.490	37.630	4.5
16	20151121_015825	20.591	38.602	4.2	61	20181108_224600	20.470	37.590	4.2
17	20151123_093002	20.581	38.517	3.9	62	20181110_021338	20.490	37.650	4.2
18	20151125_031447	20.545	38.526	4.2	63	20181111_233835	20.510	37.630	4.8
19	20151129_083609	20.613	38.722	4.1	64	20181118_060644	20.310	37.560	4.3
20	20151212_083445	21.158	37.831	4.6	65	20181119_055651	20.670	37.540	4.1
21	20160104_072145	20.401	38.315	4	66	20181129_002259	20.260	37.630	4.2
22	20160104_180055	20.591	38.603	4.3	67	20181213_062641	20.640	37.520	4.4
23	20160329_214300	20.279	37.661	3.8	68	20190115_011149	20.410	38.290	4.2
24	20160411_185344	20.332	38.213	4.3	69	20190115_012505	20.620	38.940	4.3
25	20160426_141515	21.104	37.868	3.9	70	20190117_214639	20.670	37.650	4.3
26	20160429_035053	20.605	38.696	3.9	71	20190201_050200	20.950	37.950	3.9
27	20160604_163825	20.347	38.139	4.4	72	20190205_022609	20.590	38.980	5.2
28	20160913_061449	21.204	37.775	4.1	73	20190216_015716	20.690	37.690	3.9
29	20160914_022003	20.214	37.962	3.9	74	20190306_015445	22.020	38.360	3.9
30	20161003_023443	21.196	37.765	3.9	75	20190325_062107	20.620	37.630	3.9
31	20161009_120412	20.258	38.170	3.9	76	20190328_091301	21.940	38	4.1
32	20161203_210435	21.979	38.090	4.7	77	20190416_010456	20.710	37.710	3.9
33	20170109_095316	21.718	38.336	4.5	78	20190427_232557	20.610	37.600	3.9
34	20170110_124452	21.719	38.321	4.2	79	20190513_165717	21.270	37.680	4.7
35	20170228_220201	20.152	37.902	4.1	80	20190513_212733	21.270	37.690	4.3
36	20170405_154329	21.772	38.317	4.5	81	20190521_085819	21.250	37.920	4.4
37	20170415_013446	20.506	38.385	3.9	82	20190524_211759	21.240	37.940	3.9
38	20170514_044606	21.910	38.910	4.1	83	20190619_232453	20.530	38.090	3.9
39	20170619_045537	21.200	38	4	84	20190707_222218	20.570	37.520	3.9
40	20170627_035116	20.420	38.260	3.9	85	20190713_150843	21.250	38.840	4.7
41	20170715_012203	21.990	38.340	4.1	86	20190728_050253	20.570	37.600	3.9
42	20170715_030514	22.030	38.340	4	87	20191011_224320	20.930	37.700	4.4
43	20170720_071545	21.940	38.390	4.1	88	20191012_064935	20.550	37.560	4.2
44	20170910_083154	22.110	38.010	3.8	89	20191126_044929	21.880	38.370	4
45	20170911_162015	21.530	39.150	4.9					